

Models for the Elementary Mechanical Properties of Steel Welds

H. K. D. H. Bhadeshia

University of Cambridge
Materials Science and Metallurgy
Pembroke Street, Cambridge CB2 3QZ, U. K.
www.msm.cam.ac.uk/phase-trans

Abstract. The methods now available for the computation of heat and fluid flow, solidification, microstructural and residual stress development are well advanced. It is logical therefore to proceed to the quantitative relationships between microstructure and mechanical properties so that the variety of models can be consolidated and used directly in the design process. This paper deals with a few of the important mechanical properties and describes some of the innovative treatments under development for the production of better welds or for the exploitation of welding technologies in novel applications.

INTRODUCTION

It has been possible for some time to estimate the microstructure of steel weld metals from their chemical composition and welding parameters. This is extremely useful in the development of alloys, given a broad understanding of what constitutes a good microstructure. The methodology cannot, however, be used directly in engineering design because that requires specific values of mechanical properties.

The purpose of this paper is to show that it is possible to create semi-empirical models which are useful as design tools. Such models exploit the sometimes tenuous connections between microstructure and properties. The actual design process can be quantitative or creative, the latter occasionally leading to unexpected discoveries. It is not intended here to describe the theory behind the prediction of microstructure because that can be found in recent reviews [1–13]. Attention will be focused instead on the relations between microstructure and selected mechanical properties. The latter include toughness, impurity embrittlement and parameters which inherently have a lot of scatter. Some of the important mechanical properties are described first, and then placed within the context of weld deposits. There are many difficulties in modelling mechanical properties; the role of modelling is therefore described first.

GENERAL CONCEPTS

The vast majority of welding materials that have commercial applications have been designed using accumulated experience and great skill. Any attempt to simplify this methodology via

quantitative modelling must recognise the full complexity of the microstructure and the properties that depend on it [14]. Basic science is not yet ready to tackle all the necessary problems. A range of methods must therefore be used.

Blind procedures such as, regression or neural network analysis can reveal new regularities in data. They closely mimic human experience and are capable of learning or being trained to recognize the correct science rather than nonsensical trends. Unlike human experience, these models can be transferred readily between generations and developed continuously to make design tools of lasting value. Modelling also imposes a discipline on the digital storage of valuable experimental data, which may otherwise be lost with the passage of time.

The ideal models are those based on firm physical principles. Once established, they can be used with greater confidence and are capable predicting entirely new phenomena. In materials science any attempt to model by simplification (*i.e.*, convert into a pure problem) is likely to diminish the value of the model to technology. A practically useful method is always one which is a compromise between basic science and empiricism. Good engineering has the responsibility to reach objectives in a cost and time-effective way.

The modelling approach to the design of materials and processes is important and in great demand by industry because empirical experiments are now too expensive. In a competitive environment, there may also be severe time penalties. Good modelling techniques can reduce the time from conception to production, can provide quantitative tools of lasting value, and permit a reliable and easy route for the transfer of technology between university and industry.

A design process must address all aspects in a connected way [15]. This means that each aspect of manufacture must be made amenable to modelling. The presentation that follows is, in this respect, unsatisfactory because all the necessary mechanical properties are not addressed. An attempt has nevertheless been made to demonstrate the principles involved, both for properties which lend themselves to “rigorous” treatment and others which do not.

COMPONENTS OF YIELD STRENGTH

It may be reasonable to assume that the strength of steel microstructures can be factorised into a number of intrinsic components:

$$\sigma = \sigma_{Fe} + \sum_i x_i \sigma_{SS_i} + x_C \sigma_C + K_L \{L\} + K_D \rho_D^{0.5} \quad (1)$$

where x_i is the concentration of a substitutional solute which is represented here by a subscript i . The other terms in this equation can be listed as follows:

- $K_L \{L\}$ function for strengthening due to ‘grain’ size, 115 MN m^{-1} .
- K_D coefficient for strengthening due to dislocations, $7.34 \times 10^{-6} \text{ MN m}^{-1}$.
- σ_{Fe} strength of pure, annealed iron, 219 MN m^{-2} at 300 K.
- σ_{SS_i} substitutional solute (i) strengthening.

- σ_C solid solution strengthening due to carbon.
- ρ_D dislocation density, typically 10^{16} m^{-2} .
- \bar{L} measure of the ferrite plate size, typically $0.2 \mu\text{m}$.

The individual strengthening contributions are discussed next.

PURE IRON

Pure body-centered cubic iron in a fully annealed condition makes an intrinsic (Peierls) contribution σ_{Fe} which depends on the temperature (T) and strain rate ($\dot{\epsilon}$). This dependency on T and $\dot{\epsilon}$ is most pronounced at temperatures less than about -25°C ; at higher temperatures the strength hardly varies, with only a slight decrease consistent with the temperature dependence of the elastic modulus [16; Fig. 1]. The strength then decreases sharply for temperatures in excess of 600°C ; welds in power plant operate at about 600°C and therefore have to be strengthened with highly stable precipitate phases in order to survive over a period of about 30 years, the typical design life of such plant. Experimental data for pure iron can be found in [17–19].

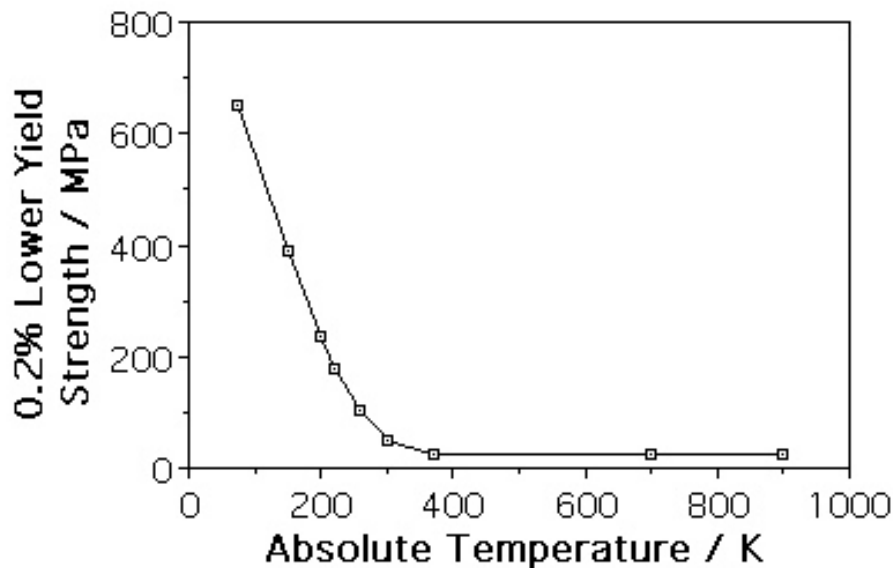


Fig. 1: Temperature dependence of the yield strength of iron (getterred with Ti) at a plastic strain of 0.2% [16]. The strain rate is about $2.5 \times 10^{-4} \text{ s}^{-1}$.

SUBSTITUTIONAL SOLUTES

Solid solution strengthening due to substitutional alloying elements is rather more complicated to treat. The elements have different solubilities in austenite and in ferrite so that they

may be distributed non-uniformly in the weld microstructure, which may in any case contain solidification-induced chemical segregation. Notwithstanding the segregation, it turns out that substitutional solutes do not in fact partition during the transformation of austenite to the variety of ferritic phases that are found in welds. This is because martensite, bainite, acicular ferrite and Widmanstätten ferrite grow by a displacive mechanism in which the lattice change is accomplished by a deformation which does not require the diffusion of iron or substitutional solutes [10,20]. The deformation is evident in the invariant-plane strain shape change (with a large shear strain) associated with the growth of each of these phases; the shape deformation also causes a lot of strain which determines the plate shape of all of these transformation products [13]. Allotriomorphic and idiomorphic ferrite, on the other hand, grow by a reconstructive transformation mechanism in which all atoms diffuse to accomplish the lattice change without much strain. Under equilibrium conditions, allotriomorphic ferrite should have a different substitutional solute concentration when compared to the alloy as a whole. However, at the large cooling rates typical of welding, even allotriomorphic ferrite seems to grow by a reconstructive mechanism in which the interface moves at a rate which traps substitutional solutes whether or not they wish to partition. This is called *paraequilibrium* [21,22,23].

In conclusion, it may reasonably be assumed that the ratio of substitutional-solute to iron atoms in ferritic phases is not different from that calculated from the composition of the steel as a whole. Solid solution strengthening contributions can therefore be estimated directly from the steel composition (assuming that carbide, nitrides and other phases do not soak up alloying elements). The strengthening contribution σ_{SS_i} can be estimated as a function of temperature and strain rate from published data, Fig. 2 [24,25].

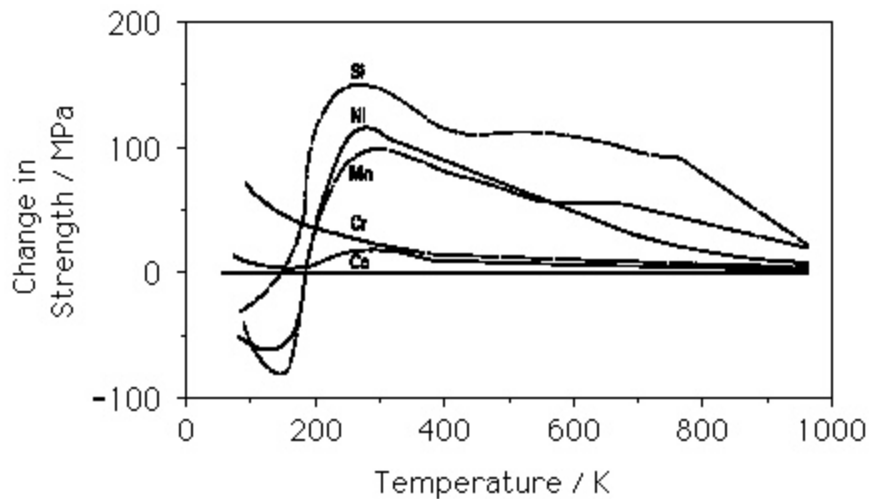


Fig. 2: The effect of some substitutional solutes (3 at.%) on the strength of otherwise pure polycrystalline iron as a function of the test temperature. After Leslie [24].

Fig. 4 shows some interesting typical data [24,25,26]: that whereas the strength of pure iron increases as the temperature is reduced, strengthening due to substitutional solutes often goes through a maximum as a function of temperature, Fig. 3. Indeed, there is some solution *softening* at low temperatures because the presence of a foreign atom locally assists a dislocation to overcome the exceptionally large Peierls barrier of body-centered cubic iron, at low tem-

peratures. Fig. 3 shows that the solid solution strengthening due to substitutional solutes may reasonably be assumed to vary linearly with concentration.

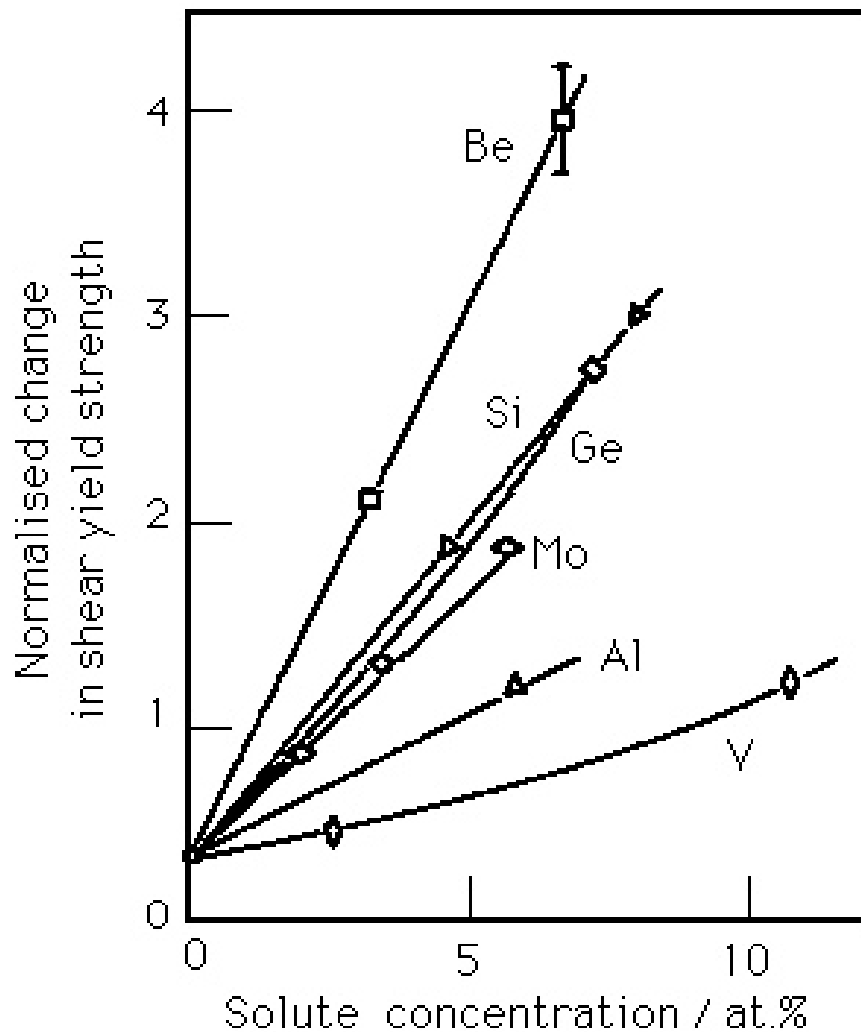


Fig. 3: The effect of some substitutional solutes on the shear yield strength of otherwise pure single-crystal iron at a temperature of 300 K. The strength increment is normalised with respect to 10^{-3} of the shear modulus. After Takeuchi [25].

It is emphasised here that the data presented in Fig. 4 are “pure”, in the sense that they are derived from very careful experiments in which the individual contributions can be measured independently. There exist a vast range of published equations in which the strength is expressed as a (usually linear) function of the weld chemistry [see for example, Table 5.2 of reference 27]. These equations are derived by fitting empirically to experimental data and consequently include much more than just solid solution strengthening components.

Use of the pure data also has the advantage that the solid solution strengthening contribution can be separated from other solute effects. For example, it has been demonstrated [10] that the influence of molybdenum in multirun steel weld deposits is far greater than expected from its solid solution strengthening; there appear to be secondary-hardening effects which are

	200 °C	100 °C	Room Temperature (23 °C)	-40 °C	-60 °C
Fe	215	215	219	355	534
Si	78	95	105	70	-44
Mn	37	41	45	8	-57
Ni	19	23	37	-2	-41
Mo	-	-	18	-	-
Cr	7.8	5.9	5.8	7.4	15.5
V	-	-	4.5	-	-
Co	1.0	1.8	4.9	9.1	5.8

Fig. 4: Strength of pure iron as a function of temperature, and solid solution strengthening terms for ferrite, for 1 wt.% of solute. The data are for a strain rate of 0.0025 s^{-1} .

prominent at concentrations greater than about 0.5 wt.%, even when precipitation cannot be observed using conventional transmission electron microscopy.

CARBON

Steels are being designed with ever decreasing interstitial contents. At the same time, processing technology allows accelerated cooling without excessive distortion or microstructural gradients. Lean steels with lower ‘carbon equivalents’ can therefore be manufactured, making fabrication relatively easy. Alloys such as these give uniform microstructures in spite of solidification-induced chemical segregation. Segregated microstructures are more susceptible to stress-corrosion and hydrogen-induced cracking. Consequently, new methods are necessary in order to calculate the microstructure and hence the mechanical properties of the heat-affected zone, the solubility of carbon in ferrite being one of the important factors.

Although the solubility of carbon in ferrite is small and often assumed to be about 0.02 wt.%, it actually changes sharply with temperature and alloy composition (Fig. 5a). The solubility illustrated is when ferrite is in equilibrium with austenite; it will be different (much smaller) when ferrite is in equilibrium with cementite or with any other carbide. The retrograde shape of the phase boundary illustrated in Fig. 5a is a consequence of the detailed thermodynamics of solution of carbon in ferrite [*e.g.*, reference 28] It means that the solubility of ferrite which is in equilibrium with austenite achieves a maximum as a function of temperature; note that the maximum solubility is not at the eutectoid temperature.

The carbon present in ferrite has a major influence on austenite formation in very low carbon steels, and hence on the subsequent development of heat-affected zone microstructures. The effect illustrated in Fig. 5b [29] is mostly thermodynamic in origin; kinetic factors are less important because both the diffusion coefficient and the driving force increase with temperature during austenite formation. The temperature at which austenite starts to form during heating is called the A_s temperature; that at which austenite formation is completed is the

A_f temperature. The slope of the A_s line (Fig. 5b), and the interval $A_f - A_s$ can be explained directly by reference to the equilibrium Fe–C phase diagram, *i.e.*, by the slope of the $\alpha/\alpha + \gamma$ phase boundary. An important observation from Fig. 5b is that very small changes in the carbon concentration of ultra-low carbon steels can have a large effect on microstructural development.

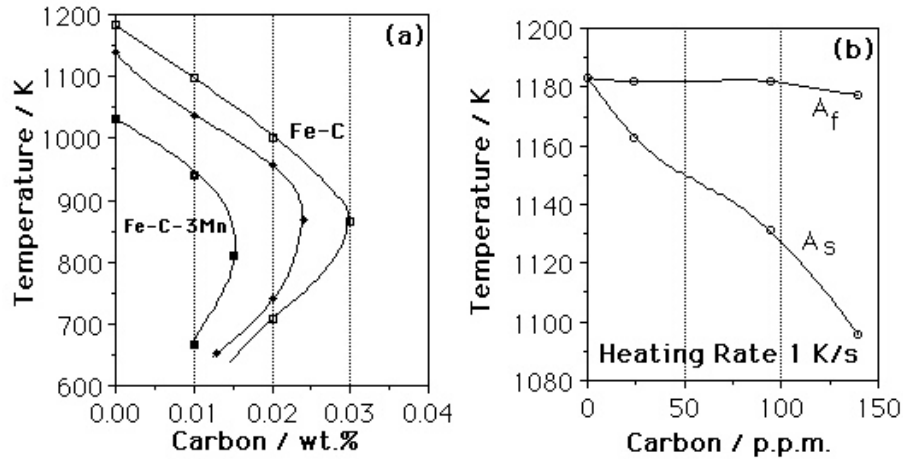


Fig. 5: (a) The $\alpha/(\alpha + \gamma)$ paraequilibrium (Ae'_1) phase boundary for Fe–C, Fe–C–1Mn and Fe–C–3Mn wt.% steels [30]. (b) Austenite–start (A_s) and austenite–finish (A_f) temperatures for Fe–C low–carbon steels [29]. Small changes in the carbon concentration have a large effect on the temperature at which austenite forms during heating of ultra–low carbon steels.

Martensite can have carbon concentrations which are well in excess of the average concentration in the alloy, because transformation at temperatures above the martensite–start temperature (M_s) changes the chemical composition of the residual austenite. The total carbon concentration in the alloy (\bar{x}) is the sum of the concentrations in the austenite (x_γ) and ferrite (x_α):

$$\bar{x} = x_\gamma V_\gamma + x_\alpha V_\alpha \quad (2)$$

where V_γ and V_α are the volume fractions of austenite and ferrite respectively. It follows that:

$$x_\gamma = \frac{\bar{x} - V_\alpha x_\alpha}{1 - V_\alpha} \quad (3)$$

x_γ is the concentration in the residual austenite before it transforms into martensite. It is this which determines the hardness of the martensite. Solid–solution theory indicates that the strength increment due to carbon dissolved in the martensite should vary with the square root of the carbon concentration [31]:

$$\sigma_{SSC} = 1722.5 \times x^{1/2} \quad (4)$$

where strength is in MN m^{-2} and the concentration x is expressed in wt.%.

DISLOCATIONS

When martensite, bainite, acicular ferrite or Widmanstätten ferrite forms at high temperatures, the shape change due to shear transformation causes plastic deformation, and hence the accumulation of dislocations in both the parent and product phases [13,20,32]. The extent of the plasticity depends on the yield strength of the parent austenite, and hence on the temperature. The dislocation density (ρ_D) of both martensite and bainite can therefore be represented empirically as a function of temperature alone (Fig. 6), for the temperature range 570–920 K [33]:

$$\log_{10}\{\rho_D\} = 9.2840 + \frac{6880.73}{T} - \frac{1780360}{T^2} \quad (5)$$

where T is the transformation temperature in Kelvin, and ρ_D is stated in units of m^{-2} . The strengthening σ_ρ (MN m^{-2}) due to dislocations is given by

$$\begin{aligned} \sigma_\rho &= 0.38\mu b(\rho_D)^{0.5} \\ &\simeq 7.34 \times 10^{-6}(\rho_D)^{0.5} \end{aligned} \quad (6)$$

where μ is the shear modulus and b the magnitude of the Burgers vector.

The empirical equation should not be used outside of the stated temperature range. However, it is sometimes necessary to calculate the dislocation density for transformation temperatures which are less than 570 K. It cannot be assumed that the dislocation density will continue to increase indefinitely as the transformation temperature decreases [34]. Instead it should stabilise at some limiting value, since any reduction in dislocation density caused by dynamic recovery effects must become negligible at low temperatures. To a good approximation, ρ_D for $T < 570$ K is given by the value at 570 K.

GRAIN SIZE

Grain boundaries are formidable obstacles to the passage of slip so it is not surprising that they cause strengthening. Stress leads to the generation and flow of dislocations within individual grains. Macroscopic yielding is said to occur when the deformation propagates across adjacent grains. This happens when concentrated stress due to the of a pile up of dislocations at a grain boundary stimulates dislocation sources in adjacent grains. The greater the number of dislocations involved in the original pile-up, the larger is the stress concentration. The number of dislocations that can participate in a pile-up increases with the size of the grain. Thus, the yield strength decreases as the grain size increases.

This is the basis of the classical Hall–Petch relation, in which the increase in strength, σ_G , caused by the introduction of a grain structure is given by:

$$\sigma_G \simeq k_{hp}(\bar{L})^{-\frac{1}{2}} \quad (7)$$

MARTENSITE COMPOSITION AND M_S TEMPERATURE

We have already seen that the growth of ferrite prior to martensitic transformation can enrich the residual austenite with carbon. The carbon concentration of the martensite that forms subsequently can be estimated using mass balance (equation 3). The martensite–start temperature (M_S) of the residual austenite can be written:

$$M_S = M_S^o - 564(x_\gamma - \bar{x}) \quad (9)$$

where the concentrations are in wt.%, the temperatures in °C, and M_S^o is the martensite–start temperature of austenite with the average composition of the alloy. Carbon is a major contributor to the strength of martensite. It causes an asymmetrical (tetragonal) distortion of the crystal structure. A distortion like this can interact strongly with both the shear and hydrostatic components of the dislocation stress–field, thereby causing considerable hardening. The lattice distortion caused by carbon in austenite is, by contrast, symmetrical, giving only a weak interaction with the hydrostatic stress–field of edge dislocations. Consequently, carbon does not greatly strengthen austenite.

TRANSFORMATION TWINS IN MARTENSITE

The Bain strain is a homogeneous pure deformation which can change the face–centered cubic crystal structure of austenite into the body–centered cubic (or tetragonal) structure of martensite. This pure deformation can be combined with a rigid body rotation to give a net lattice deformation which leaves a single line unrotated and undistorted (*i.e.*, an invariant–line strain). In a situation where the transformation is constrained, such a low degree of fit between the parent and product lattices would lead to a great deal of strain as the product phase grows.

However, by adding a further inhomogeneous lattice–invariant deformation (slip or twinning), the combination of deformations appears macroscopically to be an invariant–plane strain [38–40]. Whether the lattice–invariant deformation is slip or twinning is probably determined by kinetic factors such as the mobility of the martensite–austenite interface [41]. As a rough rule, twinned martensite tends to occur when the martensite–start temperature is relatively low.

Weld microstructures often contain small regions of austenite which are enriched with carbon and which subsequently transform to high–carbon martensite during cooling to ambient temperature. These are the so–called microphases. Transformation twins on $\{1\ 1\ 2\}_{\alpha'}$ are often found in this high–carbon martensite. This twinned martensite is frequently suggested to be responsible for bad mechanical properties. It can, however, easily be demonstrated that the twins themselves do not greatly hinder the passage of dislocations [31,40] and so are unlikely to cause any problems with toughness (Fig. 7). Dislocations can readily traverse the coherent $\{1\ 1\ 2\}_{\alpha'}$ twin boundaries body–centered cubic or body–centered tetragonal lattices. It was at one time believed that the twins were responsible for the high strength of ferrous martensites, because the numerous twin boundaries should hinder slip. This is incorrect because twinned martensites which do not contain carbon are not particularly strong. It is now generally accepted that the strength of virgin ferrous martensite is largely due to interstitial solid solution hardening by carbon atoms, or in the case of lightly autotempered martensites due to carbon atom clustering

or fine precipitation. Consistent with this, it is found that Fe-30Ni wt.% twinned martensites are not hard.

In conclusion, any detrimental effect of the twinned martensite present in the microphases is unlikely to be due to the twins *per se*, but rather the very high carbon concentration which makes the untempered martensite brittle.

Although glide across coherent twin boundaries in martensite should be unhindered, the boundaries will cause a small amount of hardening. Corresponding slip systems in the matrix and twin will in general be differently stressed because they are not necessarily parallel [31,42]. Work is also needed to create the steps in the interfaces (Fig. ??). It is emphasized, however, that these should be very minor contributions to the strength of martensite in the microphases found in weld deposits.

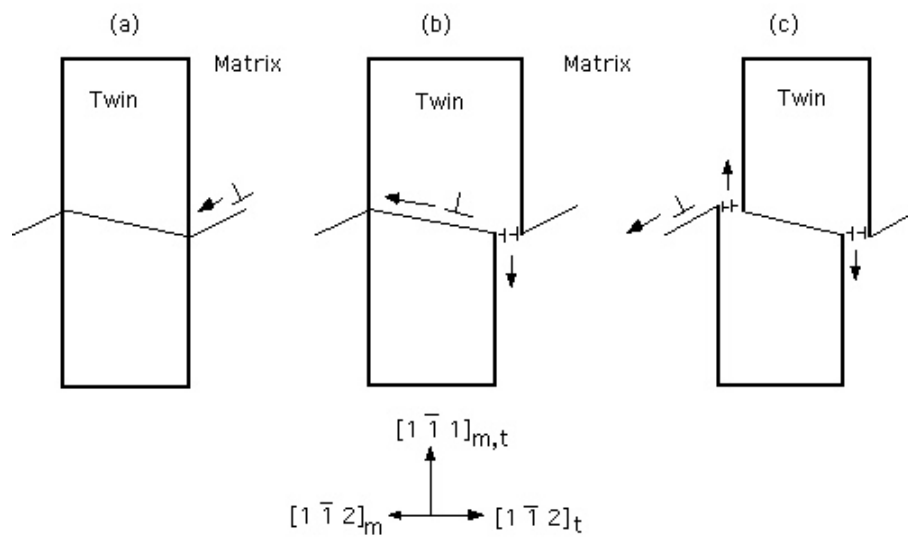


Fig. 7: The passage of a slip dislocation across a coherent twin boundary in a body-centred cubic crystal structure. The subscripts m and t refer to the matrix and twin respectively. The twinning system is $(\bar{1} 1 2)[1 \bar{1} 1]$, with a shear strain $s = 2^{-1/2}$. (a) Matrix dislocation of Burgers vector $\frac{a}{2}[\bar{1} 1 1]$ is about to enter the twin. (b) Matrix dislocation has penetrated the twin and changed its Burgers vector $\frac{a}{2}[1 \bar{1} \bar{1}]$, and left behind a step defined by dislocations, each of Burgers vector $\frac{a}{6}[\bar{1} 1 \bar{1}]$. (c) Dislocation leaves twin and enters the matrix, recovering its original Burgers vector $\frac{a}{2}[\bar{1} 1 1]$, and leaving a further step defined by dislocations, each of Burgers vector $\frac{a}{6}[\bar{1} 1 1]$

STRENGTH OF MIXED MICROSTRUCTURES

The normal way to calculate the strength of a multiphase alloy is to use a rule of mixtures, *i.e.*, to estimate a mean value from the weighted average of each component:

$$\sigma = V_{\alpha}\sigma_{\alpha} + V_{\beta}\sigma_{\beta} + \dots \quad (10)$$

This approximation may not always be valid in circumstances where the phases have very different mechanical properties. This is because of constraint effects and the need to conserve mass between product phases with different chemical compositions [34].

The constraint effect can be explained as follows. It is well established in fracture mechanics that the yield strength is increased by plastic constraint. This is why a weak brazing alloy can be used to bond much stronger samples, as long as the thickness of the braze material is small enough to be constrained throughout by the surrounding stronger matrix. Indeed, the strength of the joint increases as the thickness of the braze layer decreases (Fig. 8).

Dispersions of bainite plates grow in austenite which subsequently transforms to much stronger martensite. This is similar to the brazing analogy. The deformation of the bainitic ferrite can therefore be expected to be constrained by the harder martensite. This can be modelled using experimental data available from brazed joints in high strength steels. As already discussed, the brazing alloys used in making the joints were non-ferrous materials which are ordinarily rather weak. The data, in a normalised form, are summarised in Fig. 8. The vertical axis is the joint strength normalised with respect to that of the unconstrained braze material; the horizontal axis is the braze thickness normalised relative to a thickness value where the restraint effect vanishes.

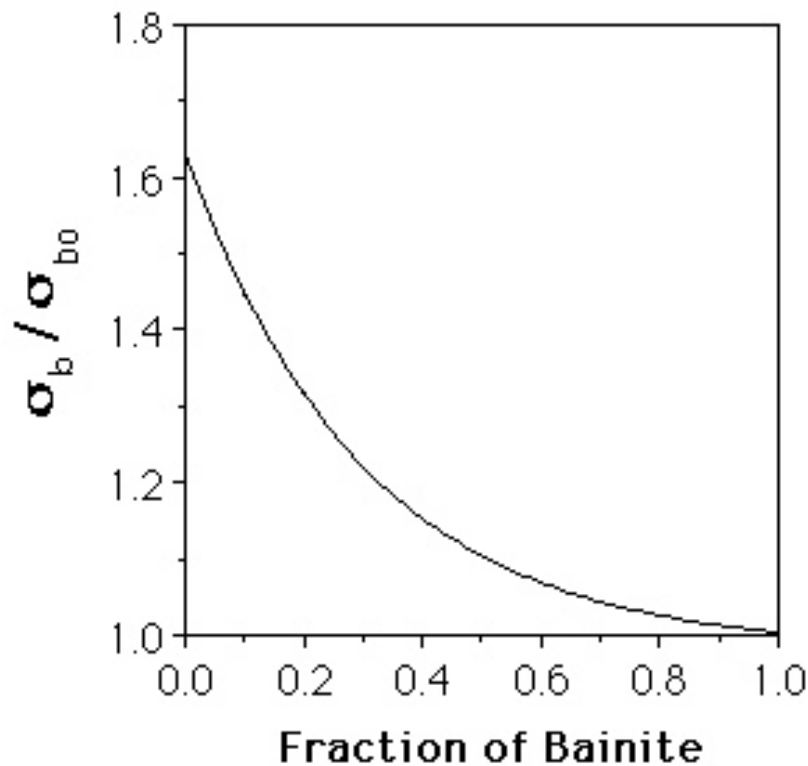


Fig. 8: Plot of the normalised strength of a brazed joint versus the normalised thickness of the brazing material, the latter being identified with the fraction of bainite in a martensitic matrix [34].

To analyse the properties of a mixed microstructure of martensite and bainite, it can be assumed that the normalised braze thickness is equivalent to the volume fraction of bainite. Using this

assumption, and the form of the normalised strength versus normalised thickness plot (Fig. 8), the strength of constrained bainite may be represented by the equation:

$$\sigma_b \simeq \sigma_{b0}[0.65 \exp\{-3.3V_b\} + 0.98] \leq \sigma_M \quad (11)$$

where σ and σ_0 represent the strengths of constrained and unconstrained bainite respectively, σ_M is the strength of the martensite and V_b is the volume fraction of the bainite. The strength of bainite is always less than or equal to that of martensite.

When the volume fraction V_b of bainite is small, its strength nearly matches that of martensite (Fig. 9), always remaining above that of bainite on its own. The strength of martensite continues to increase with the fraction of bainite, as the carbon concentration of the residual austenite from which it grows, increases.

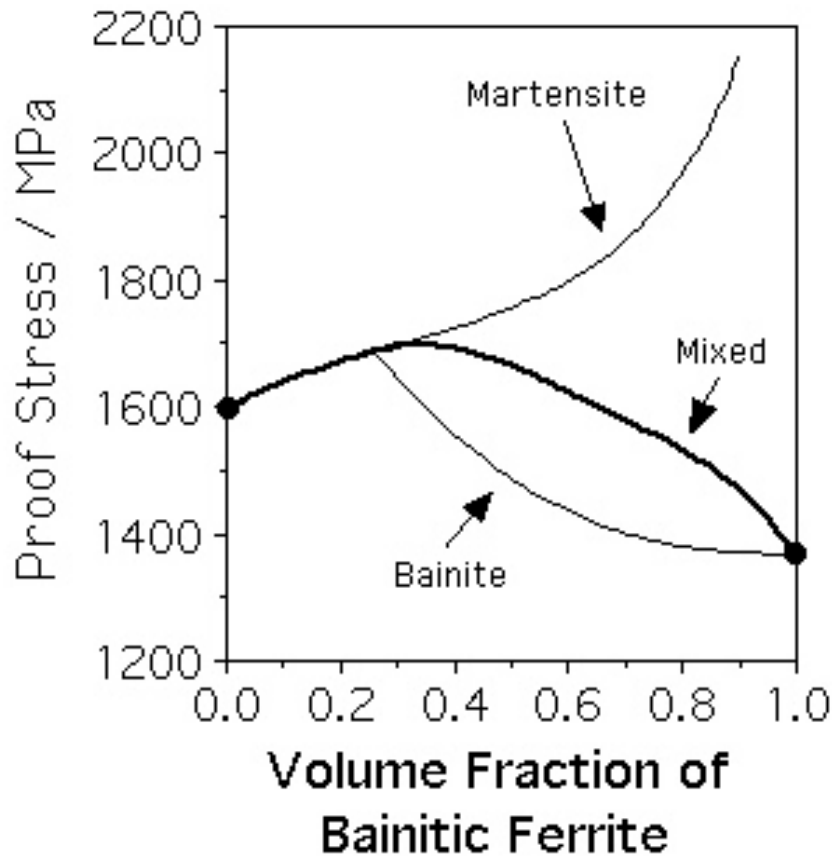


Fig. 9: The strength contributions of bainite and martensite in the mixed microstructure which has been tempered [34].

Fig. 10 shows a comparison between experimental and calculated data for the strength of the mixed microstructure. Line (a) on Fig. 10 shows that a rule-of-mixtures cannot account properly for the variations observed. The agreement between calculation and experiment improves (curve b) as allowance is made for the change in the strength of martensite as carbon partitions

into the austenite, due to the formation of bainite. The consistency between experiment and theory becomes excellent as constraint effects are also included in the calculations (curve c).

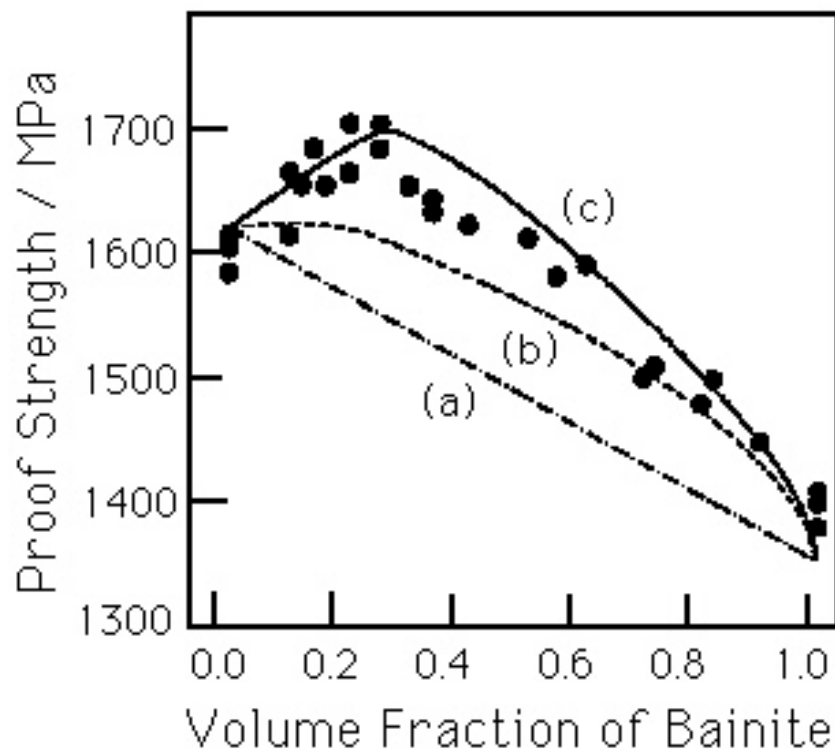


Fig. 10: Comparison of the measured [43–46] strength of a mixed microstructure of tempered bainite and tempered martensite, against calculations for a variety of approximations [34].

Constraint effects are of important in determining the mechanical behaviour of weld microstructures in many respects. Hrivnak [47] has indicated that hard-phase islands present in the heat-affected zone microstructures are most detrimental when they are severely constrained by the surrounding microstructure. Since the constraint is expected to be larger when the island is relatively small, it is these small islands which act as local brittle zones. This is discussed in detail in the section on local brittle zones.

STRENGTH OF ACICULAR FERRITE

An example calculation of the different factors which contribute to the strength of acicular ferrite is presented in Fig. 10a. The most important contribution other than the intrinsic strength of featureless iron, is the small effective ‘grain size’ of acicular ferrite. As discussed earlier, the mean free slip distance in a plate of acicular ferrite is determined more than anything else by its thickness. It is necessary to consider therefore, the factors which determine the thickness and aspect ratio (*i.e.*, thickness to length ratio) of acicular ferrite plates.

Acicular ferrite is a displacive transformation [10]. The shape deformation associated with a displacive transformation in steel can be described as an invariant-plane strain with a relatively

large shear component. Christian [48] demonstrated that when the shape strain is elastically accommodated, the strain energy scales with the plate aspect ratio. This is why all of the displacive transformation products in steel, *e.g.*, Widmanstätten ferrite, bainite, acicular ferrite and martensite, occur in the form of thin plates.

The need to minimise strain energy demands a thin plate, but this also leads to a minimisation of the volume of transformation per plate. Therefore, a plate will tend to adopt the largest aspect ratio consistent with the available free energy change driving the transformation. In ideal circumstances, where the transformation interface remains glissile throughout, and where there is no friction opposing the motion of the interface, *thermoelastic equilibrium* occurs [32,49,50,51]. The aspect ratio of the plate adjusts so that the strain energy is equal to the driving force, as illustrated in Fig. 10b. The driving force is increased by cooling the austenite, which should lead to plates of increased thickness. Alternatively, it can be decreased by the addition of austenite stabilising elements such as carbon or manganese.

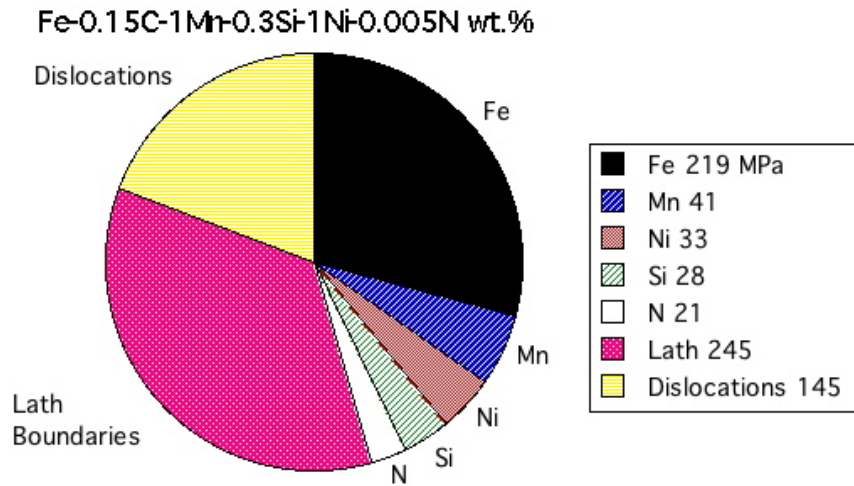
There are good experimental observations [52,53] which have been interpreted recently [54] to support the idea that an increase in the acicular ferrite plate thickness continues until the chemical driving force is exhausted by the accumulation of strain energy. The isolated plates of acicular ferrite which nucleate from point inclusion sites are free to increase in thickness even when their increase in length is restricted by other platelets growing from other inclusions. It is found experimentally that the aspect ratio of acicular ferrite decreases as the transformation temperature is raised, or as the manganese or carbon concentration is increased [52,53].

The idea of thermoelastic equilibrium can therefore be applied to acicular ferrite even though acicular ferrite is probably not entirely elastically accommodated in the matrix. There is thus an easy method for calculating the changes in the acicular ferrite grain size using thermodynamics, an important result given the large grain size strengthening contribution illustrated in Fig. 10a.

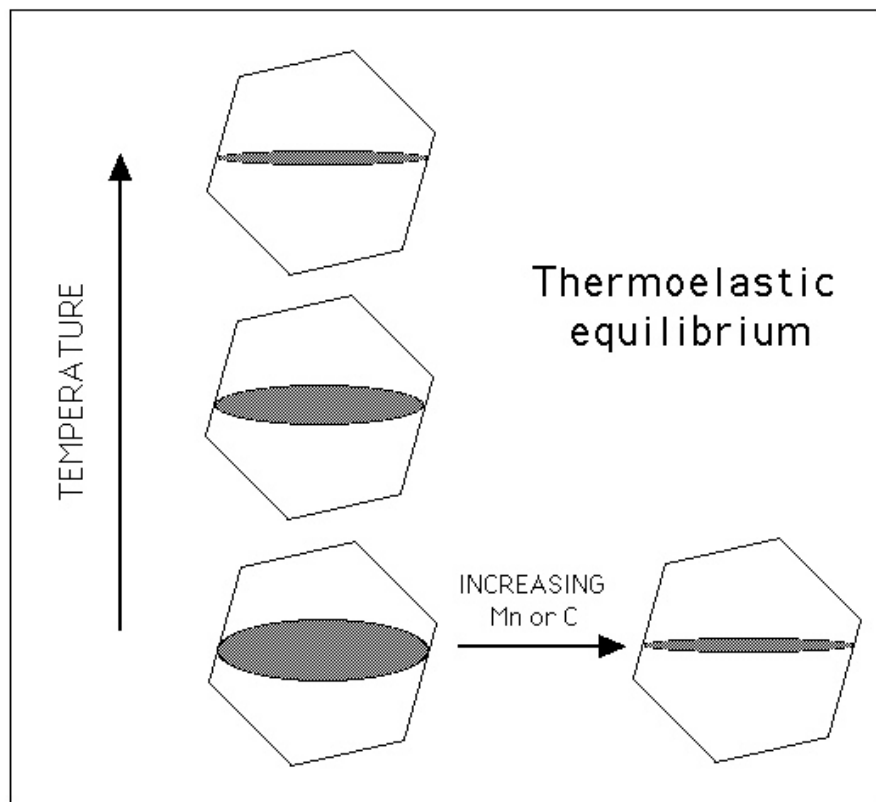
Dislocations also make a significant contribution, but the extent of dislocation strengthening will, unlike the lath size effect, decrease as the transformation temperature increases. Notice that the substitutional solutes make only small contributions to the strength of ferrite. This may be surprising at first sight, since many regression equations describing the strength of welds have much larger coefficients for these solutes. However, those equations do not refer to the solid solution strengthening alone, but to all the effects including for example, any changes in the microstructure caused by alloying. Carbon is not included in Fig. 11 a since its solubility in the ferrite is negligible.

MULTIRUN WELDS

It has been demonstrated that some reasonable assumptions can be made to simplify the calculation of the strength of multirun weld deposits [55]. A volume fraction V_P is defined to include both the primary microstructure [10], and the reheated regions which are *fully* austenitised, on the grounds that these regions are mechanically similar to the as-deposited regions. The remainder $V_S = 1 - V_P$, includes all the regions which have been tempered or partially austenitised, and which have lost most of the microstructural component of strengthening. V_P can be estimated from the alloy chemistry since this in turn influences the extent of the austenite phase field via the Ae_3 temperature [56,57]. It is emphasised that V_P and V_S do not refer to



(a)



(b)

Fig. 11: (a) Factorisation of the strength of acicular ferrite in a weld of typical chemical composition. These data are calculated as described in the text, and refer to a hypothetical microstructure which contains only acicular ferrite. (b) Effect of thermoelastic equilibrium on aspect ratio of plate of fixed length [54].

the volume fractions of the primary and secondary microstructures respectively, but are defined in a peculiar way to simplify the task of estimating the strength of multirun welds. Thus, V_P includes the primary microstructure and regions which are fully austenitised by the deposition of further material, and V_S includes all the other regions which have essentially lost most of the microstructural component of strength [56,57].

The yield strength σ_Y of a multirun MMA weld deposit is given by:

$$\sigma_Y = V_P\sigma_P + V_S\sigma_S \quad (12)$$

where σ_P is the yield strength of the primary microstructure, assumed to equal that of the reheated regions which are fully reaustenitised. σ_S is the yield strength of regions which have largely lost the microstructural component of strength, and which are either partially reaustenitised or tempered. Recent work has resolved σ_P into components due to the strength of pure, annealed iron σ_{Fe} , solid-solution strengthening components σ_{SS} and microstructural strengthening components σ_α , σ_{α_w} and σ_{α_a} , due to α , α_w and α_a respectively [55]. Similarly, σ_S has been resolved into σ_{Fe} , σ_{SS} and a component due to microstructural strengthening. Hence, both σ_P and σ_S can be estimated from a knowledge of the volume fractions of phases, alloy chemistry and readily available data on the strength of iron.

Fig. 12 shows a series of calculations in which the weld composition is progressively enriched with austenite stabilising elements. Apart from the expected enhancement of strength, increased alloying leads to the following further consequences:

- (i) There is an increase in the ratio of the yield to ultimate tensile strength (Fig. 12). In high strength steels it is desirable to have a proof stress to UTS ratio (r_1) which is less than about 0.8. This helps to ensure that there is substantial plastic deformation prior to ductile fracture. A low value of r_1 in many cases correlates with good fatigue resistance. Steel columns used in the construction of high-rise buildings in earthquake areas are required to absorb energy without failure, requiring a low value of r_1 . Too low a value can also lead to difficulties. Pipe lines used for the conveyance of oil or gas under pressure have to undergo a pre-service hydrotest in which the pipe is pressurised to 125% of the planned service pressure. If the value of r_1 is too small, then there is a danger of gross plastic deformation during hydrotesting. Consequently, the r_1 ratio has to be greater than 0.85 for pipe applications [58].
- (ii) There are variations in the microstructure of multirun welds and consequent inhomogeneities in strength as a function of position. The mean yield strength is close to the minimum for lean alloys, whereas it is closer to the maximum yield strength for richly alloyed welds. Lean alloys have a generally soft microstructure with a small quantity of harder regions and vice versa for the richly alloyed welds. Thus, the microstructure of multirun welds is most homogeneous for the extremes of alloying.
- (iii) It is intriguing that there are regions of the weld metal microstructure which have a yield strength that is less than the ultimate tensile strength (Fig. 12). Bearing in mind that the UTS is a nominal rather than a true stress, it is likely that all regions of the weld metal have yielded prior to failure. However, the distribution of strains is expected to be inhomogeneous.

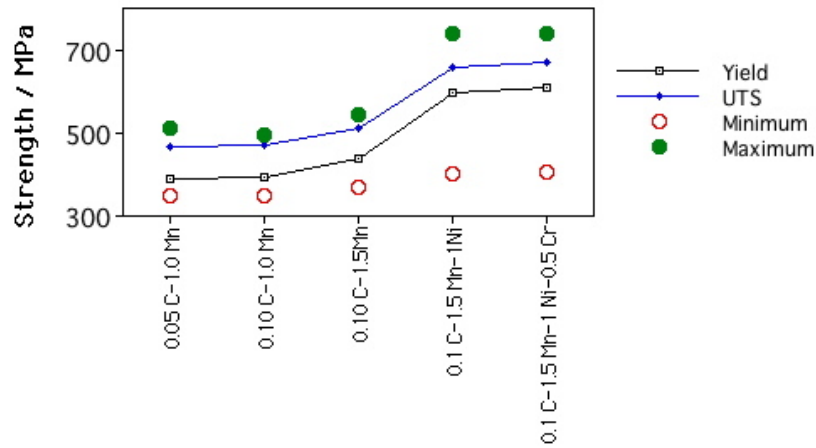


Fig. 12: Calculated variations in microstructure and mechanical properties as a function of the chemical composition (wt.%) of steel welds deposited using the manual metal arc welding (1 kJ mm^{-1}). Each weld also contains 50 parts per million by weight of nitrogen and 300 parts per million by weight of oxygen. The interpass temperature used for the calculations was $100 \text{ }^\circ\text{C}$. The minimum and maximum values are for the yield strength.

Fig. 13 shows the calculated variations in the strength of submerged-arc all weld metal deposits made with a heat input of about 4 kJ mm^{-1} . There is a systematic variation in the carbon concentration for so-called carbon-manganese welds containing a variety of other additions. The columnar austenite grain size \bar{L}_{tn} [10] was calculated as a function of the heat input, the carbon, silicon and manganese concentrations as follows:

$$L_{tn} = 154.6 - 2228C - 10.56Si + 33.77Mn - 0.1133 \times \text{oxygen} + 0.5604 \times Q \quad (13)$$

where \bar{L}_{tn} is in μm , the concentrations of all elements are in wt.% (with the exception of oxygen which is in parts per million by weight) and the heat input has units of J m^{-1} . The equation is limited to maximum concentrations of C, Mn and Si being 0.152, 1.93 and 0.4 respectively; when the concentrations exceeded these limits, they were assumed to be given by the appropriate limit for the purposes of grain size estimation.

The data in Fig. 13a show that the overall yield and tensile strengths become virtually insensitive to the carbon concentration because of the major effect of carbon on the austenite grain size. The decrease in hardenability accompanying any reduction in the carbon concentration is virtually compensated by the increase in hardenability due to a larger austenite grain size. It is believed that the effect of carbon on the austenite grain size comes in via its effect on the δ -ferrite to austenite transformation. The columnar austenite grains grow directly from the columnar δ -ferrite grains. Carbon increases the driving force for $\delta \rightarrow \gamma$ reaction, thereby promoting an increase in the nucleation rate of austenite, leading to a refinement of the grain size.

Fig. 13b shows how the strength might have varied with the carbon concentration at a fixed austenite grain size. The intuitively expected trend, that the strength increases with carbon concentration is indeed observed in that case. It is noteworthy that the difference in the strengths of the weakest and strongest regions now increases with the carbon concentration.

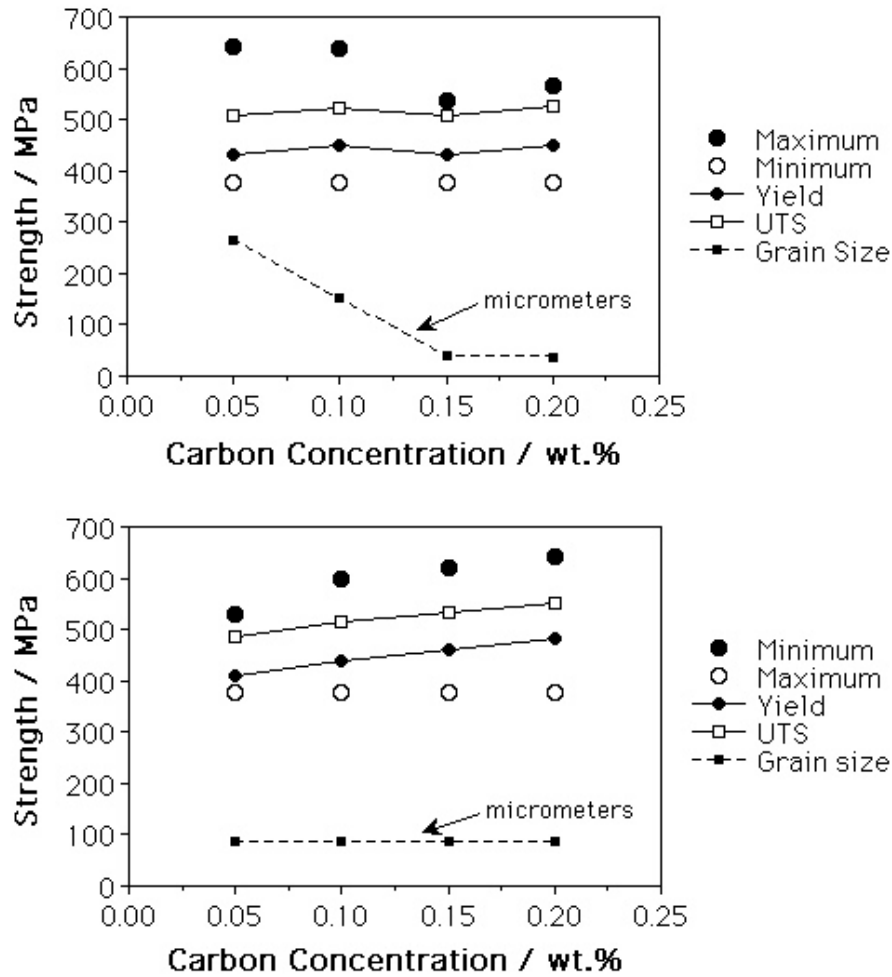


Fig. 13: Calculated variations in the strength of submerged arc welds made using a current of 550 A, 32 V, 0.004 m s^{-1} , of composition Fe-C-0.3Si-1Mn-0.03Al-0.03Ti-0.005S wt.%, in addition to 500 p.p.m.w. of oxygen and 50 p.p.m.w. of nitrogen. The interpass temperature used for the calculations was $100 \text{ }^\circ\text{C}$. The minimum and maximum values are for the yield strength. (a) These calculations include expected variations in the columnar austenite grain size (\bar{L}_{tn} , μm). (b) These calculations are based on a fixed austenite grain size.

The effects of manganese and nickel are illustrated in Fig. 14. The sensitivity to carbon concentration increases as the manganese concentration is increased (Fig. 14a). The addition of nickel is not as effective as that of manganese in changing the strength. A comparison of the change in strength of the 1.5Mn alloy, when a further 1 wt.% of manganese is added to the case where a further 1 wt.% Ni is added shows that the increase is much greater in the former case. This is because manganese has a much larger effect on the hardenability of steel.

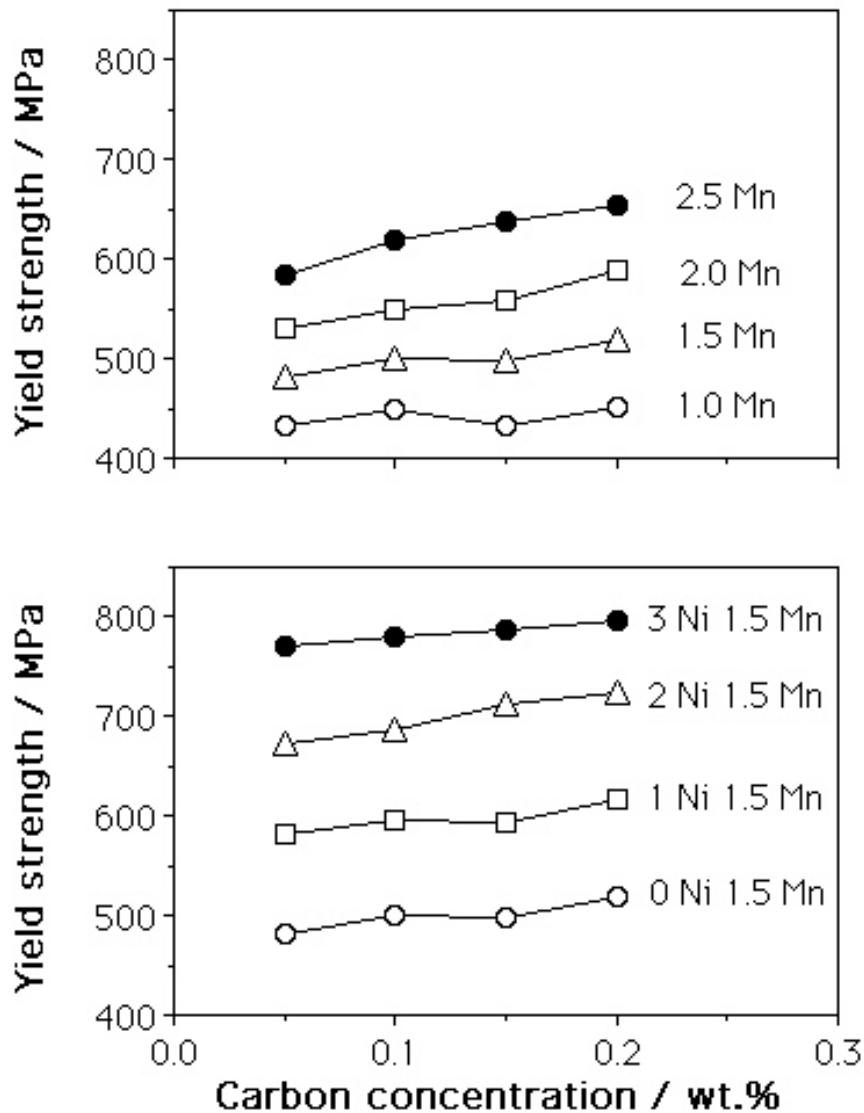


Fig. 14: Calculated variations in the strength of submerged arc welds made using a current of 550 A, 32 V, 0.004 m s^{-1} , of base composition Fe-C-0.3Si-0.03Al-0.03Ti-0.005S wt.%, in addition to 500 p.p.m.w. of oxygen and 50 p.p.m.w. of nitrogen. The interpass temperature used for the calculations was 100°C . The minimum and maximum values are for the yield strength. (a) The effect of variations in the manganese concentration. (b) The effect of variations in the nickel concentration when the manganese is fixed at 1.5 wt.%.

DUCTILITY

There has been a limited amount of progress in the modelling of tensile ductility of the as-deposited microstructure of steel welds [59]. The ductility can to a good approximation be divided into two main components whose magnitudes are assumed to be controlled by different physical processes. These components are the uniform plastic strain, as recorded prior to the onset of macroscopic necking in the tensile specimen, and the nonuniform component which is the remainder of the plastic strain.

By factorising the ductility into these components, it is possible to express the nonuniform component in terms of the inclusion content of the weld deposit, after taking into account variations in specimen cross-sectional area (A_O) and gauge length (L_O):

$$\text{nonuniform elongation, \%} = 100 \times \beta \frac{A_O^{0.5}}{L_O} \quad (14)$$

where β is Barba's constant, but now expressed as a function of the inclusion content:

$$\beta \simeq 1.239 - 9.372 \times (\text{wt.\% O}) + (\text{wt.\% S}). \quad (15)$$

There is as yet no model for estimating the uniform component of strain, but such a model would require a detailed knowledge of the strain hardening behaviour of the individual phases of the microstructure, together with some theory for multiphase deformation. Note that the equation emphasises the role of particles in reducing ductility.

QUANTITATIVE MODELS FOR FRACTURE TOUGHNESS

Much of the literature about mechanical toughness tends to focus on micromechanisms, test methodology or procedures for using experimental data in design exercises. By contrast, there is very little work on the prediction of the ability of complex engineering materials to absorb energy during fracture. This difficulty is illustrated by some basic concepts of fracture mechanics. The critical value K_{IC} of the stress intensity which must be exceeded to induce rapid crack propagation is the product of two terms [60]:

$$K_{IC} = \text{stress} \times \text{distance}^{\frac{1}{2}} \quad (16)$$

where the stress is a fracture stress σ_F which can be measured independently using notched tensile specimens. It can be related to the microstructure via [61,62]:

$$\sigma_F \propto \left[\frac{E\gamma_p}{\pi(1-\nu^2)c} \right]^{\frac{1}{2}} \quad (17)$$

where E is the Young's modulus and ν is the Poisson's ratio. γ_p is the effective work done in creating a unit area of crack plane, estimated to be about 14 J m^{-2} for many iron-base microstructures [60]; it is much larger than a surface energy (typically 1 J m^{-2}) because of the plastic zone which moves with the crack tip. This value of 14 J m^{-2} seems to apply to a wide variety of steel microstructures [60], which is surprising given that they often have quite different deformation characteristics. In any event, there is no obvious way of relating γ_p to details of the microstructure. By contrast, the dimension c is usually attributed to the size of a sharp crack created by the fracture of a brittle microstructural constituent such as a cementite particle in wrought steels, or a non-metallic inclusion in a weld deposit.

The other parameter in the equation, $\text{distance}^{\frac{1}{2}}$, refers to a distance ahead of the crack tip, within which the stress is large enough to cause the fracture of brittle crack-initiators. It is well-defined for coarse microstructures but not for many useful microstructures.

The temperature dependence of the fracture toughness of steels seems to be very well-behaved. Wallin [63,64] has shown that the shape of the toughness versus temperature curve is virtually the same for all structural steels, making it possible to define a universal dependence as follows:

$$\Delta K = 77 \exp\{0.019(T - T_0)\} \quad \text{MPa m}^{1/2} \quad (18)$$

where ΔK is a change in toughness due to a corresponding change in temperature T . T_0 is a “transition temperature” where the fracture toughness for a 25 mm thick specimen is $100 \text{ MPa m}^{1/2}$. There is no reason to believe that such an equation should not apply to weld metals. It would, of course, be necessary in each case to determine the T_0 temperature experimentally.

To summarise, there are excellent concepts of fracture mechanics, with established relationships between parameters such as stress and crack-dimensions. These same relationships cannot be used predictively because in each application they rely on experimental data. It is nevertheless true that there is a good qualitative understanding of the factors that control toughness. There are modelling methods which can help convert these qualitative notions into quantitative relationships. These are discussed below in the context of Charpy toughness.

THE CHARPY TOUGHNESS

A test used to characterise toughness is the Charpy test, in which a square sectioned, notched bar is fractured under specified conditions [65]. The energy absorbed during fracture is taken as a measure of toughness. The Charpy test is empirical in that the data cannot be used directly in engineering design. It is nevertheless a useful quality control test which is specified widely in international standards, and in the ranking of samples in research and development experiments.

The toughness of a steel depends on many variables, and that of a weld on many more because of the complexity of the welding process. It is not yet possible to predict the Charpy toughness of a weld with any reliability. The usual approach is to correlate the results against chosen variables using linear regression analysis [*e.g.*, reference 66]. These methods are known to be severely limited in their application.

Therefore, the most important mechanical property for welds has not been rationalised quantitatively as a function of the complex array of variables associated with welding. However, it is known from experience, and from the concepts of fracture mechanics, that certain variables are more important than others in their effect on toughness. Given this experience, it should be possible to train an artificial neural network to estimate weld toughness quantitatively as a nonlinear function of these variables, and to see whether the patterns that emerge from the work emulate metallurgical expectations.

In normal regression methods the analysis begins with the prior choice of a relationship (usually linear) between the output and input variables. A neural network is capable of realising a greater variety of nonlinear relationships of considerable complexity. Data are presented to the network in the form of input and output parameters, and the optimum non-linear relationship is found by minimising a penalized likelihood. The network in effect tries out many kinds of

relationships in its search for an optimum fit. As in regression analysis, the results then consist of a specification of the function, which in combination with a series of coefficients (called weights), relates the inputs to the outputs. The search for the optimum representation can be computer intensive, but once the process is completed (*i.e.*, the network trained) the estimation of the outputs is very rapid. In spite of its apparent sophistication, the method is as blind as regression analysis, and neural nets can be susceptible to overfitting.

However, much of this danger can in principle be minimised or eliminated by combining the neural network approach with sound statistical and metallurgical theory [67,68,69]

Variables affecting Charpy toughness

It is possible to choose a set of variables which should, using experience of welding metallurgy, have an influence of the Charpy toughness of weld metal. These variables are listed in Table 2 together with their typical values for high-quality manual metal arc and submerged arc welds.

Variable	Range	Mean	Standard Deviation
Process	Submerged Arc Manual Metal Arc		
Yield Strength MPa	347–645	471	12.7
Carbon wt.%	0.029–0.13	0.08	0.004
Silicon wt.%	0.28–1.14	0.49	0.05
Manganese wt.%	0.77–2.50	1.32	0.07
Phosphorus wt.%	0.008–0.028	0.015	0.001
Sulphur wt.%	0.002–0.017	0.010	0.0005
Aluminium wt.%	0.001–0.04	0.014	0.002
Nitrogen p.p.m.w.	26–119	67	4
Oxygen p.p.m.w.	234–821	412	30
Primary Microstructure %	0–91	34	4
Secondary Microstructure %	9–100	66	2
Allotriomorphic Ferrite %	16–62	31	2
Acicular Ferrite %	11–81	55	2
Widmanstätten Ferrite %	0–35	14	2
Temperature K	213–293	259	25
Charpy Toughness J	4–215		

Fig. 15: The variables. The abbreviation p.p.m.w. stands for parts per million by weight.

In general, the toughness decreases as the strength increases. This is because plastic deformation, which is the major energy absorption mechanism during fracture, becomes more difficult as the strength increases. Hence, the yield strength is included as a variable. The nature of the welding process itself may have a significant effect on toughness. For example, the submerged arc welding process is quite different from the manual metal arc welding process, leading to the development of different microstructures and variations in impurity content. However, heat input *per se* is not included since its effect is via the microstructure, which is included in detail in the analysis.

The major solute additions to steels, *i.e.*, C, Mn and Si, have large effects on the transformation behaviour and strength. Impurity elements (P, S, Al, N, O) are included because of their known tendency to embrittle or because of their importance in the formation of nonmetallic inclusions in welds.

All fusion welding processes involve the deposition of a small amount of molten steel within a gap between the components to be joined. When the steel solidifies, it welds the components together. The *fusion zone* represents both the deposited metal and the parts of the steel component melted during the process, and is a solidification microstructure, often called the *primary microstructure* [10]. In practice, the gap between the components to be joined has to be filled by a sequence of several weld deposits. These multirun welds have a complicated microstructure. The deposition of each successive layer heat-treats the underlying microstructure. Some of the regions of original primary microstructure are reheated to temperatures high enough to cause the reformation of austenite, which during the cooling part of the thermal cycle transforms into a different microstructure. Other regions may simply be tempered by the deposition of subsequent runs. The microstructure of the reheated regions is called the *reheated* or *secondary* microstructure. The fractions of the primary and secondary microstructures are included as input variables (Table 2).

In addition, the details of the primary microstructure are also included in the list of input variables, since the phases involved (allotriomorphic, Widmanstätten and acicular ferrite) are known to have a major influence on the weld properties.

Iron undergoes a ductile–brittle transition as a function of temperature. The flow stress of iron is sensitive to temperature, the strength increasing as the temperature decreases. At some critical temperature, it becomes easier to cleave iron without expending much energy. Below this critical temperature, the iron behaves in a very brittle manner. Hence, the test temperature is included as an important variable.

All of these input variables should to varying degrees influence the Charpy toughness, which is the output variable.

The structure of a typical network used for the analysis is illustrated in Fig. 16.

Linear functions of the inputs x_j are operated on by a hyperbolic tangent transfer function:

$$h_i = \tanh\left(\sum_j w_{ij}^{(1)} x_j + \theta_i^{(1)}\right) \quad (19)$$

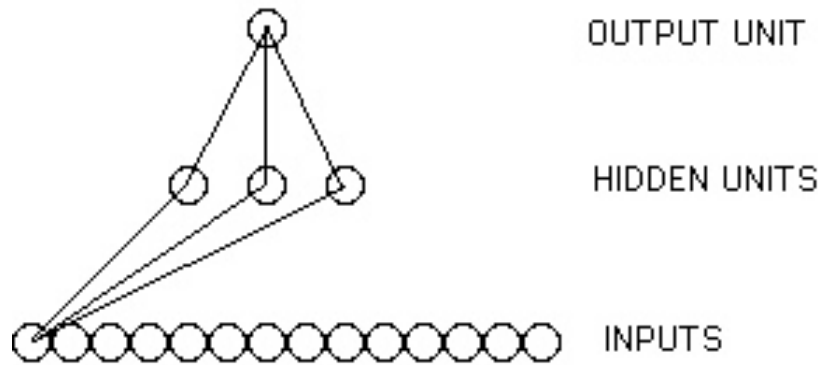


Fig. 16: A typical network used in the analysis. Only the connections originating from one input unit are illustrated, and the two bias units are not illustrated.

so that each input contributes to every hidden unit. The bias is designated θ_i and is analogous to the constant that appears in linear regression. The strength of the transfer function is in each case determined by the weight w_{ij} . The transfer to the output y is linear:

$$y = \sum_i w_i^{(2)} h_i + \theta^{(2)} \quad (20)$$

This specification of the network structure, together with the set of weights is a complete description of the formula relating to the inputs to the output. The weights are determined by training the network; the details are described elsewhere [67,68]. The training involves a minimisation of the regularised sum of squared errors. The term σ_ν used below is the framework estimate of the noise level of the data.

The complexity of the model is controlled by the number of hidden units (Fig. 16), and the values of the 16 regularisation constants (σ_w), one associated with each input, one for biases and one for all weights connected to the output.

Fig. 17 shows that the inferred noise level decreases monotonically as the number of hidden units increases. However, the complexity of the model also increases with the number of hidden units. A high degree of complexity may not be justified, and in an extreme case, the model may in a meaningless way attempt to fit the noise in the experimental data. MacKay [67,68] has made a detailed study of this problem and has defined a quantity (the *evidence*) which comments on the probability of a model. In circumstances where two models give similar results over the known dataset, the more probable model would be predicted to be that which is simpler; this simple model would have a higher value of 'evidence'. The evidence framework was used to control the regularisation constants and σ_ν . The number of hidden units was set by examining performance on test data. A combination of Bayesian and pragmatic statistical techniques were therefore used to control the model complexity. Four hidden units were found to give a reasonable level of complexity to represent the variations in toughness as a function of the input variables. Larger

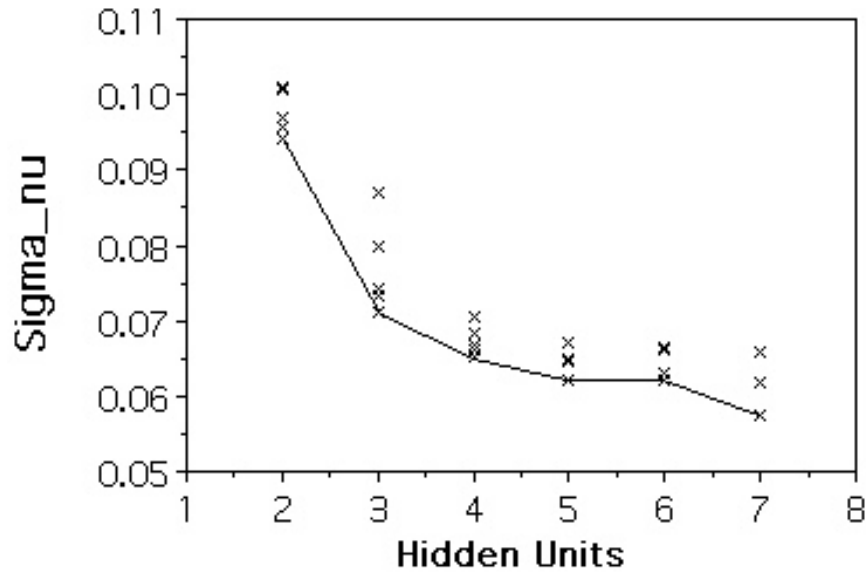


Fig. 17: Variation in σ_ν as a function of the number of hidden units. Several values are presented for each set of hidden units because the training for each network was started with a variety of random seeds.

numbers of hidden units did not give significantly lower values of σ_ν ; indeed, the test set error goes through a minimum at four hidden units (Fig. 18).

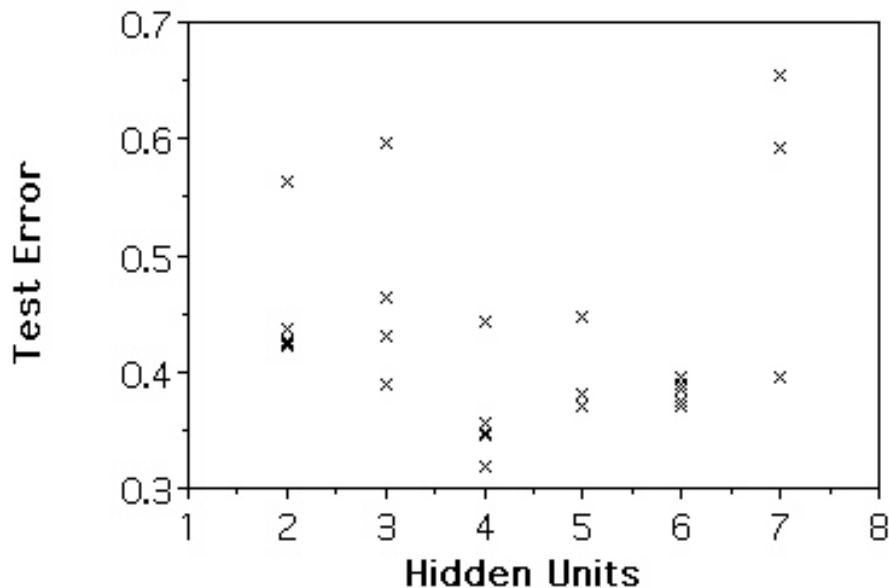


Fig. 18: The test error as a function of the number of hidden units.

The optimum parameters for one trained network are presented later in Table 3; this listing would be required in order to reproduce the predictions described, though not the error bars. The levels of agreement for the training and test datasets are illustrated in Fig. 19, which show good prediction in both instances. It should be emphasized that the test data were not included

in deriving the weights given in Table 3 (except to choose the solution displayed), so that the good fit is established to work well over the range of data included in the analysis.

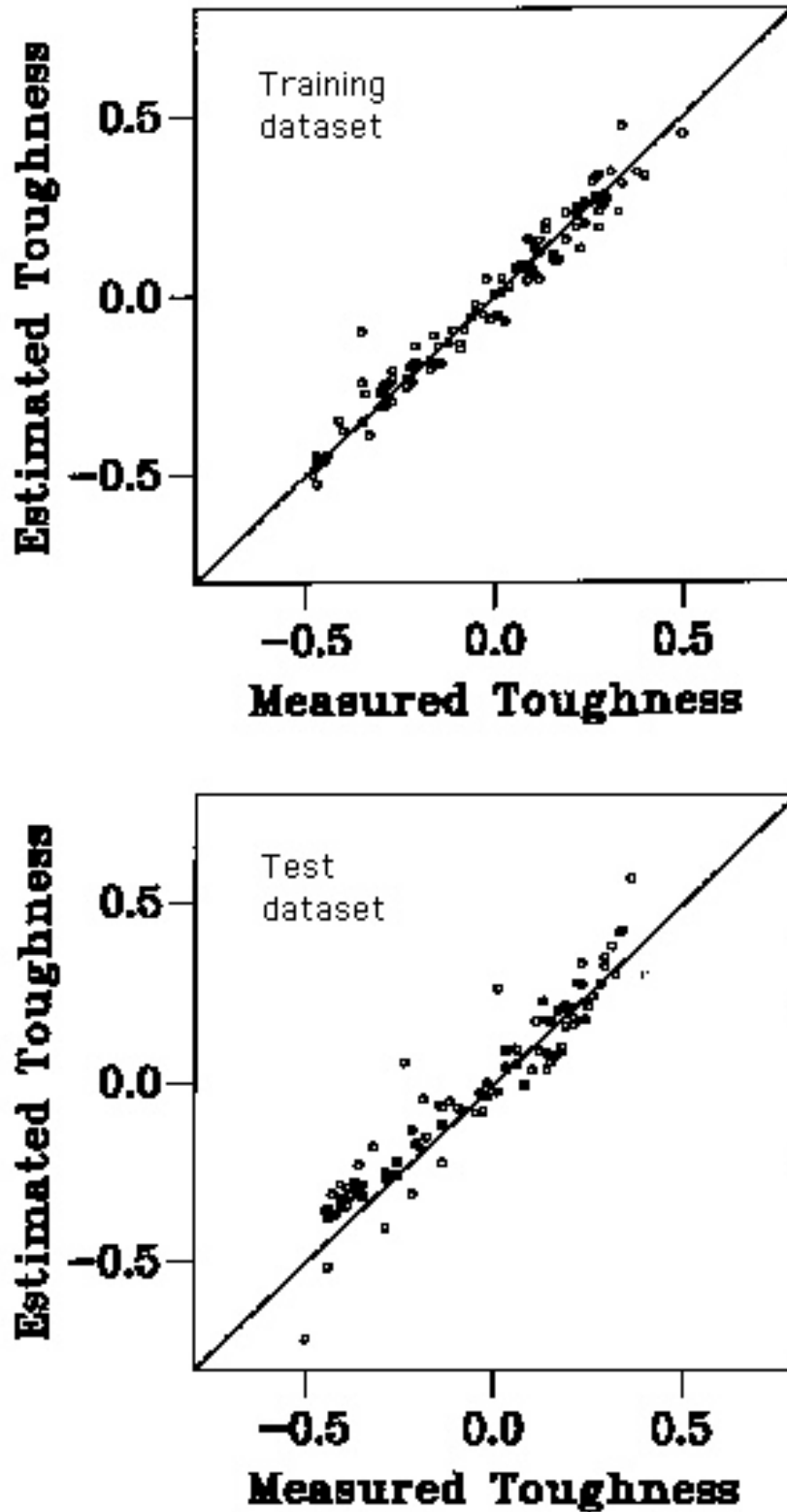


Fig. 19: Plot of the estimated versus measured toughness; (a) training dataset; (b) test dataset.

Some Predictions of Charpy Toughness

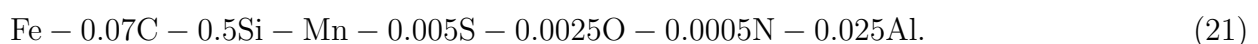
We now examine the metallurgical significance of the results [69]. We attempt predictions out of the range of the experimental data used during training, and examine some aspects which cannot be studied experimentally.

Fig. 20 illustrates the significance (σ_w) of each of the input variables, as perceived by the neural network, in influencing the toughness of the weld. The process clearly has a large intrinsic effect, which complies with experience in that submerged arc welds are in general of a lower quality than manual metal arc welds. Note that this is a process effect which is independent of all the other variables listed. The yield strength has a large effect and that is well established [65]. It is also widely believed, as seen in Fig. 20, that ferrite has a large effect on the toughness. Nitrogen has a large effect, as is well established experimentally [70–75]. Oxygen influences welds in both beneficial and harmful ways, *e.g.*, by helping the nucleation of acicular ferrite or contributing to fracture by nucleating oxides.

It is surprising at first sight that carbon has such a small effect, but what the results really demonstrate is that the influence of carbon comes in via the strength and microstructure. Phosphorus and sulphur have only a small effect; the toughness measured was in the as-welded condition whereas many of the classical embrittlement effects manifest themselves in the stress-relieved condition. It is also possible that the effects of P and S are higher at strength levels larger than encountered here. All of the welding consumables are commercially used so that they are not expected to be embrittlement prone. Elements such as Mn and Si do not feature greatly presumably because their effect comes in via microstructure. Fig. 20 also shows a relatively small effect of temperature on toughness, but it should be noted that the temperature range considered is only 80 °C, and that a part of the effect of temperature is to alter the yield strength, which is identified by the model to be one of the important variables.

The model can be used to estimate the toughness if all of the inputs listed in Table 2 are available. The amount of work required to accumulate these inputs is not trivial, but the situation can be ameliorated. A physical model [10] based on phase transformation theory can be used to predict the values of all the inputs from a knowledge of just the chemical composition and a choice of welding conditions. This was done particularly to examine the effects of carbon and manganese on weld toughness, given that a lot of work on these lines has already been reported in the literature.

Fig. 21 a shows data generated using the neural network but with all the inputs other than manganese calculated using our weld model [10]. In all cases, the calculated inputs are for manual metal arc welds with 180 A, 34 V, a welding speed of 0.004 m s⁻¹, interpass temperature 200 °C, ISO2569 weld geometry. The manganese variations are for a basic composition



It is interesting that the toughness at relatively high temperatures decreases as the manganese concentration is increased. This upper shelf region involves ductile failure, and an increase in strength leads to a reduction in the ductile fracture energy. The calculated yield strength increases from 403–539 MPa as the Mn concentration is changed from 0.5–2.0 wt.%. However, the cleavage toughness at low temperatures clearly increases with Mn up to a concentration of

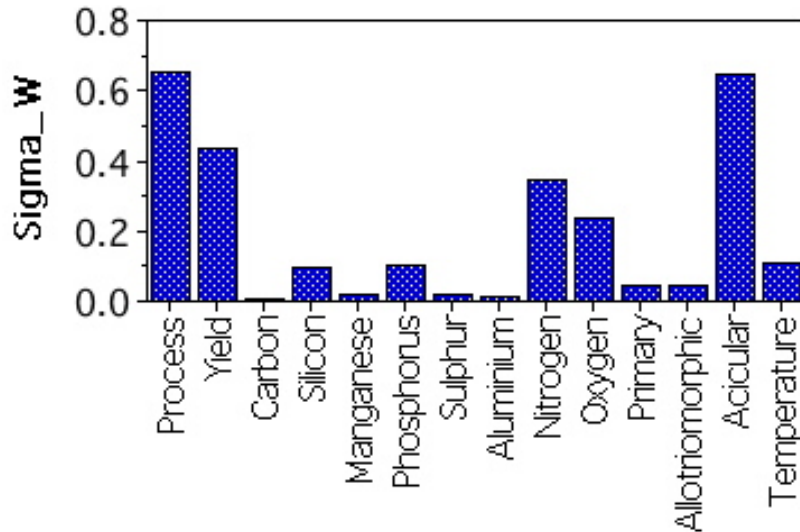


Fig. 20: Bar chart showing a measure of the model-perceived significance of each of the input variables in influencing toughness. The significance is comparable to the partial correlation coefficient of multiple regression analysis.

1.5 wt.%. This is because the calculated acicular ferrite content increases from 35-67% when Mn is changed over the range illustrated. The low temperature toughness for 2 wt.% Mn is nevertheless lower than that for the 1.5 wt.% alloy presumably because the increased acicular ferrite content is not sufficient to compensate for the increased strength. Indeed, an optimum manganese concentration of about 1.5 wt.% has been reported to achieve the best toughness in manual metal arc welds of the type discussed here [76,77].

Fig. 21b shows similar data for carbon (the only difference being that the Mn concentration is fixed at 1 wt.%). The explanation is identical to that for the Mn data.

For welds similar to the carbon series, but with the carbon concentration fixed at 0.07 wt.%, the oxygen concentration alone was varied to a range well outside of the training dataset. These results are presented in Fig. 22 along with the ± 1 standard deviation predicted error bars. It is clear that any attempt to extrapolate beyond the dataset on which the model is based gives predictions which are not terribly useful. The fact that the toughness increases with oxygen at low concentrations is strange since the acicular ferrite content (and indeed all the other inputs) are kept constant. An increase in the oxygen content alone should lead to a deterioration in toughness because of the tendency for non-metallic oxide particles to initiate fracture.

Finally, it is possible using the model to examine effects which cannot easily be produced experimentally. It has frequently been argued that acicular ferrite is a better microstructure than Widmanstätten ferrite, because the former with its less organised arrangement of ferrite plates has a greater capacity to deflect cracks. This was tested for a manual metal arc weld containing 0.07 wt.% carbon but of otherwise identical composition to the carbon series of welds (Fig. 6). The allotriomorphic ferrite fraction was set to zero and all inputs except acicular ferrite and Widmanstätten ferrite were varied in a complementary fashion. The results (Fig. 23) are

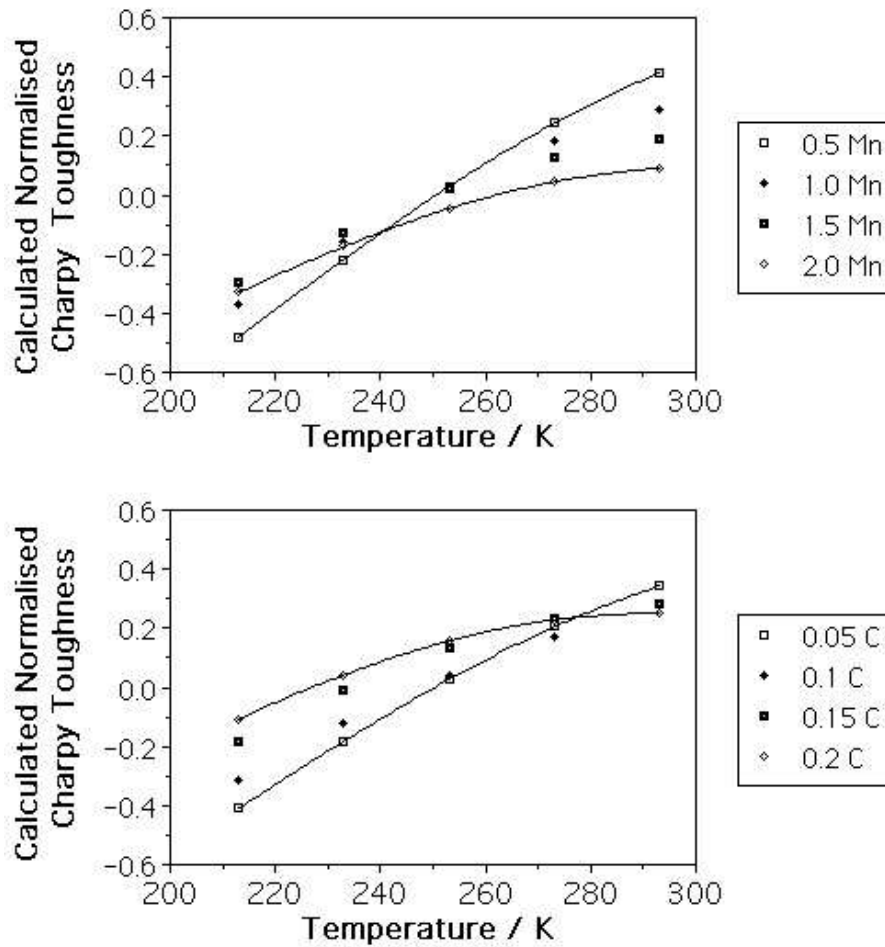


Fig. 21: (a) Variation in the normalised toughness as a function of the manganese concentration. (b) Variation in the normalised toughness as a function of the carbon concentration.

exciting – they demonstrate that increased acicular ferrite leads to an improvement of cleavage toughness but not of the upper shelf energy – the latter is not expected to change since the strengths of acicular and Widmanstätten ferrite are virtually identical [59].

Use of Charpy Neural Network

Table 3 contains the values for the weights obtained after completing the training of the network. These data can be used in combination with Table 2 and equations 19,20 in order to use the network to make predictions of weld metal toughness.

ALLOTRIOMORPHIC FERRITE

It has been accepted for some time that allotriomorphic ferrite (α) is bad for weld metal toughness because it offers little resistance to cleavage crack propagation. However, this kind of

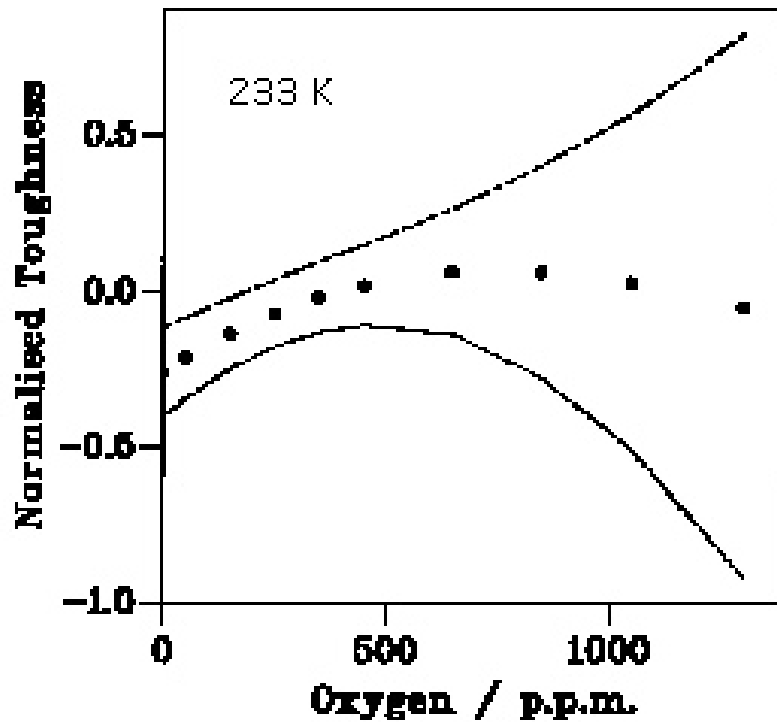


Fig. 22: Variation in the normalised toughness as a function of the oxygen concentration. Oxygen is varied here without changing any of the other inputs. The oxygen concentration in the training data was in the range 234–821 p.p.m.

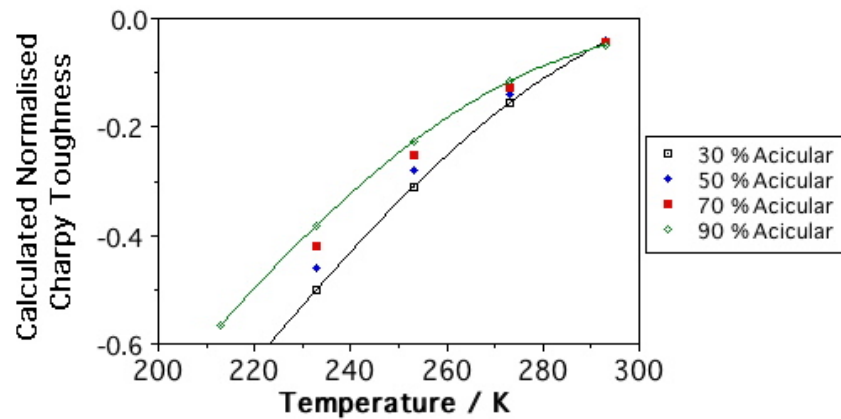


Fig. 23: Variation in the normalised toughness as a function of the acicular ferrite/Widmanstätten ferrite content, everything else being kept constant.

ferrite grows by a reconstructive mechanism in which all of the atoms diffuse. Thus, grains of α can grow freely across austenite grain boundaries. Displacive transformations (Widmanstätten ferrite, bainite, acicular ferrite, martensite) on the other hand, involve the coordinated motion of atoms. Such movements cannot be sustained across grain boundaries. Hence, in a fully transformed microstructure, a vestige of the austenite grain boundary remains when the trans-

-0.139995	-0.953784	0.599265	0.003035	-0.052339	-0.00995051	-0.108883	-0.00489392
0.00315774	0.305801	-0.00864967	0.0121499	0.0257695	-0.0740189	-0.0778886	-0.248802
0.4557	-0.396398	0.000652394	0.0699645	-0.00622593	0.0705528	-0.00814623	0.00414627
0.123011	0.0517809	-0.020293	-0.018466	0.623779	-0.0778589	0.589258	0.0100171
-0.195621	0.0029131	-0.0883861	-0.0105864	0.0295194	-0.00630463	0.00141565	-0.533206
0.333115	-0.0445803	0.0161306	0.655171	0.138927	-0.08014	0.355382	-0.0515694
0.00413126	0.0390746	-0.00848546	0.0475089	-0.0094849	0.00577479	0.028576	-0.204586
0.00875236	0.0284252	-0.748358	0.084853	-1.04271	7.47417	6.71492	7.72748
8.83568							

Table 3: The weights for the Charpy model. The data are arranged in a continuous horizontal sequence in the following order:

$$\begin{aligned} &\theta_1^{(1)}, w_{1,1}^{(1)} \dots w_{1,22}^{(1)}, \\ &\theta_2^{(1)}, w_{2,1}^{(1)} \dots w_{2,22}^{(1)}, \\ &\theta_3^{(1)}, w_{3,1}^{(1)} \dots w_{3,22}^{(1)}, \\ &\theta_4^{(1)}, w_{4,1}^{(1)} \dots w_{1,22}^{(1)}, \\ &\theta^{(2)}, w_1^{(2)} \dots w_4^{(2)} \end{aligned}$$

formation is displacive. In the presence of impurities, this can lead to intergranular failure with respect to the prior austenite grain boundaries. With allotriomorphic ferrite, the original γ boundaries are entirely disrupted, removing the site for the segregation of impurities. This conclusion is supported by observations reported in the literature. Abson [78] examined a large set of weld deposits. Of these, a particular weld which had no allotriomorphic ferrite content and a particularly high concentration of phosphorus exhibited brittle failure at the prior columnar austenite grain boundaries in the manner illustrated in Fig. 24.

It is well known that the post-weld heat treatment (600 °C) of titanium and boron containing welds leads to embrittlement with failure at the columnar austenite grain boundaries [79-81]. Phosphorus has been shown to segregate to these prior austenite boundaries and cause a deterioration in the toughness. The titanium and boron make the welds sensitive to post-weld heat treatment because they prevent allotriomorphic ferrite, and hence expose the remains of the austenite grain boundaries to impurity segregation.

Kayali *et al.* [82] and Lazor and Kerr [83] have reported such intergranular failure, again in welds containing a fully acicular ferrite microstructure. Sneider and Kerr [84] have noted that such fracture appears to be encouraged by excessive alloying. Boron is important in this respect because it can lead to an elimination of austenite grain boundary nucleated phases; recent observations on intergranular fracture at the prior austenite boundaries [85] can be interpreted in this way. This is consistent with our hypothesis, since large concentrations austenite-stabilising elements tend to reduce the allotriomorphic ferrite content.

It must be emphasised that it is not the reduction in allotriomorphic ferrite content *per se* which worsens the properties; the important factor is the degree of coverage (and hence disruption)

of the prior austenite grain surfaces. In addition, the impurity content has to be high enough to cause embrittlement. Classical theory suggests that additions of elements like molybdenum should mitigate the effects of impurity controlled embrittlement, although such ideas need to be tested for the as-deposited microstructure of steel welds. To summarise, it is likely that allotriomorphic ferrite should not entirely be designed out of weld microstructures, especially if the weld metal is likely to contain impurities.

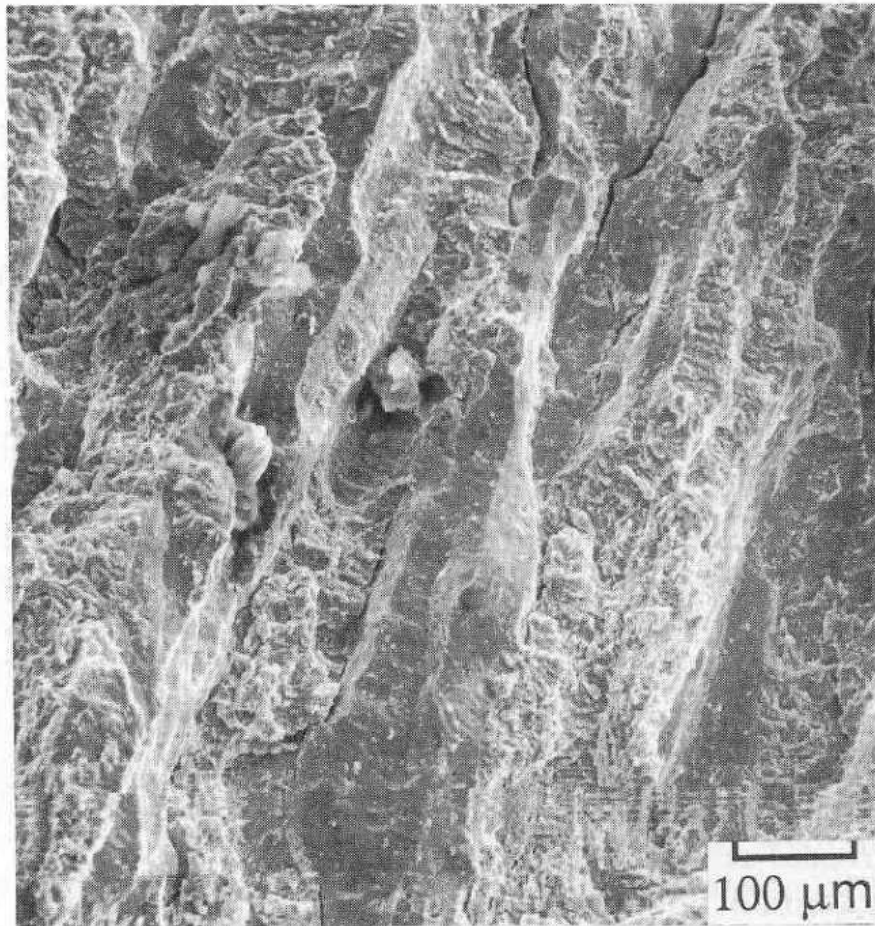


Fig. 24: Fracture along the prior columnar austenite grain boundaries in a weld with zero allotriomorphic ferrite content.

Recent work reinforces the conclusion that some allotriomorphic ferrite should be retained in the weld microstructure in order to improve its high temperature mechanical properties. Ichikawa *et al.* [86] examined the mechanical properties of large heat input submerged arc welds designed for fire-resistant steels. They demonstrated that the high temperature ductility and the creep rupture life of the welds deteriorated sharply in the absence of allotriomorphic ferrite (Fig. 25). The associated intergranular fracture at the prior austenite grain boundaries, became intragranular when allotriomorphic ferrite was introduced into the microstructure.

Steel can be infiltrated at the prior austenite grain boundaries by liquid zinc. In a study of the heat-affected zone of steel welds, Iezawa *et al.* [87] demonstrated that their susceptibility to liquid zinc embrittlement depended on the allotriomorphic ferrite content, which in turn varied with the boron concentration (Fig. 26). The absence of allotriomorphs at the prior austenite

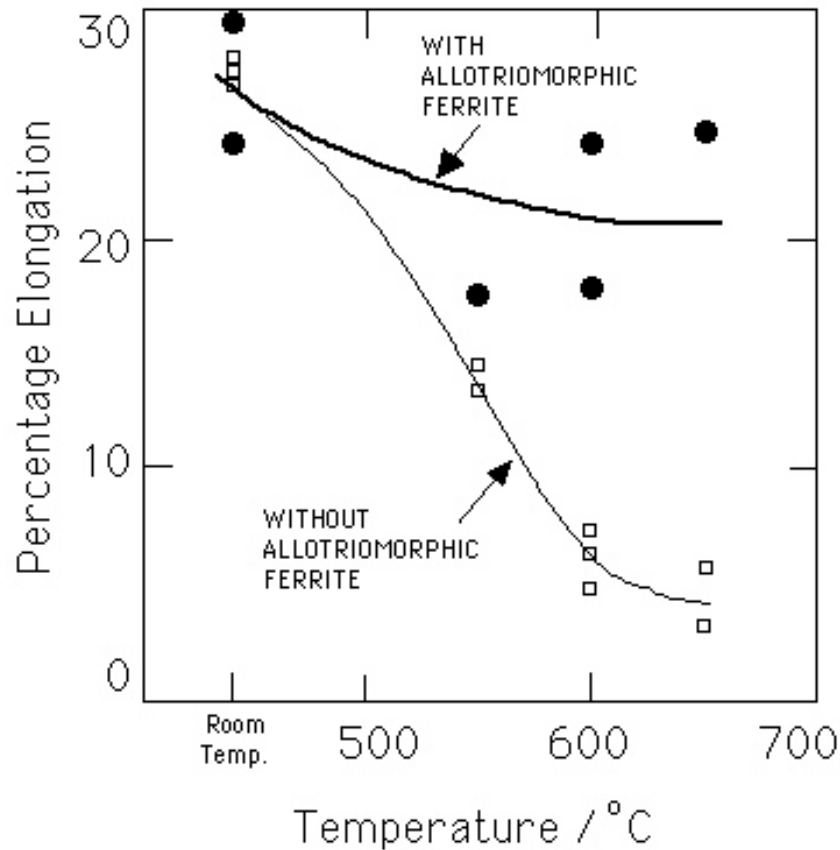


Fig. 25: The elevated temperature tensile elongation of submerged arc steel welds, in which the small amount of allotriomorphic ferrite was controlled using boron additions [86].

grain boundaries clearly made them more sensitive to zinc infiltration, proving again that these prior boundaries have a high-energy structure which is susceptible to wetting and impurity segregation.

The rutile based electrode systems currently under development generally lead to phosphorus concentrations of about 0.010–0.015 wt.%, and the popular use of titanium and boron gives a weld deposit without allotriomorphic ferrite. The welds have therefore been found to be extremely susceptible to stress relief embrittlement with fracture along the prior austenite grain boundaries. Possible solutions include:

- (a) Reduction in the phosphorus concentration, although this might entail cost penalties.
- (b) Introduction of between 0.2–0.5 wt.% of molybdenum. Molybdenum is an element frequently added to wrought steels in order to prevent impurity induced embrittlement [*e.g.*, 88]. Molybdenum has been shown to retard temper embrittlement [89–91] and retardation is greatly increased when vanadium is also added [92]. It was believed at one time that molybdenum scavenges phosphorus, but experiments have failed to confirm this mechanism [93]. Elements such as molybdenum and vanadium must be used cautiously in weld deposits, because their addition leads to a considerable increase in strength, which

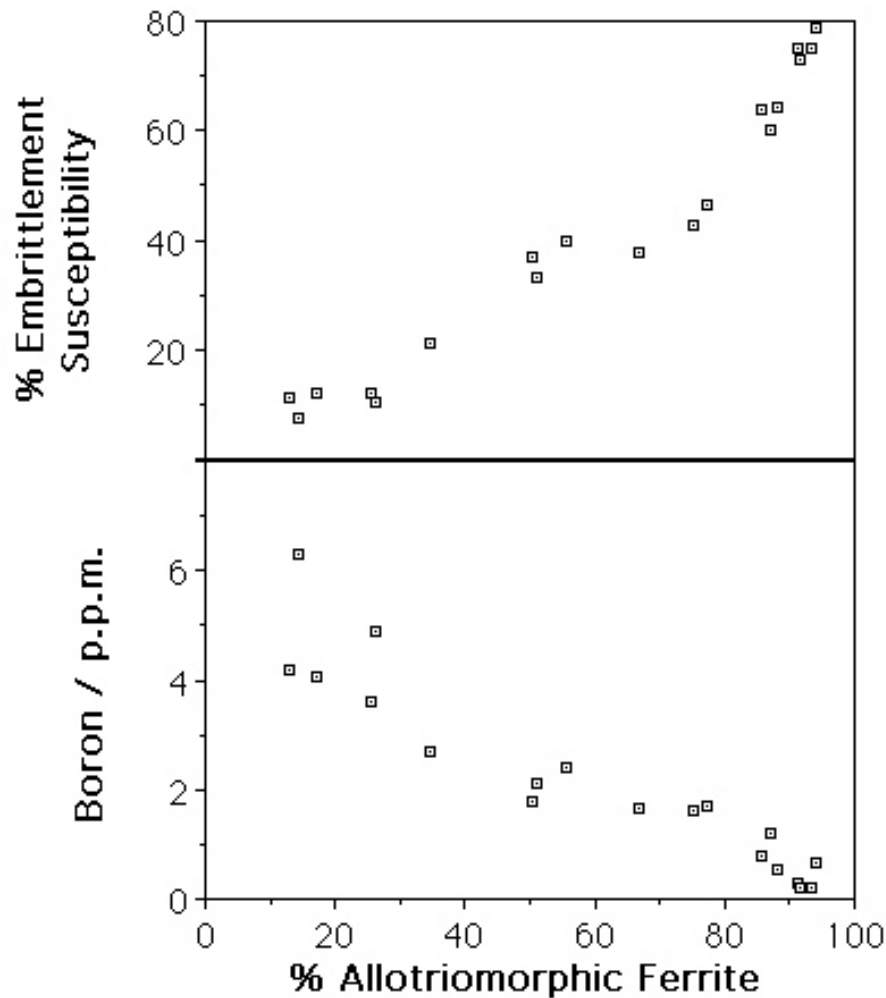


Fig. 26: Variation in the sensitivity to liquid zinc embrittlement as a function of the allotriomorphic ferrite content in the heat-affected zone of a steel weld. The diagram also shows how the allotriomorphic ferrite content was varied using boron as an alloying addition. [87].

can in turn trigger a corresponding reduction in toughness. Their use must therefore be compensated by appropriate adjustments in the concentrations of other elements.

- (c) Manganese has long been known to make steels more sensitive to impurity induced temper embrittlement [94], even in pure iron [95]. Nickel has a similar effect when silicon is also present. This suggests that both manganese and nickel concentrations should be kept to a minimum.
- (d) Carbon is known to be beneficial for intergranular cohesion [88,96]. Many cored wire electrodes have been developed to give very low carbon concentrations (0.03 wt.%) in the weld deposits. From work in the general area of welding, a carbon concentration in the range 0.10–0.12 wt.% may in fact be acceptable.

- (e) The composition of the weld should be adjusted to permit the formation of a thin layer of allotriomorphic ferrite. During transformation, the ferrite grows across the austenite grain boundaries and destroys them as potential sites for impurity segregation.

PRIOR AUSTENITE GRAIN BOUNDARIES

It was argued above that with displacive transformations (which cannot cross austenite grain boundaries), a “vestige” of the austenite grain boundary structure is left in the microstructure. The following evidence suggests that these *prior* austenite grain boundaries are high-energy boundaries:

- (a) The prior austenite grain boundaries are sites for the reversible segregation of misfitting impurity atoms such as phosphorus [88]. The extent of segregation is larger than that at martensite lath boundaries.
- (b) Carbides nucleate preferentially at the prior austenite grain boundaries during the tempering of martensite or bainite. This applies to both cementite [97] and to those alloy carbides such as $M_{23}C_6$ which find it difficult to nucleate [98]. A consequence of this is that the carbides located at the prior boundaries are coarser. Some carbides such as cementite are brittle and hence assist the propagation of fracture at the prior austenite grain boundaries.
- (c) Prior austenite grain boundaries can be revealed by etching [99], often with great clarity, in microstructures where the transformation products do not grow across austenite grains. The prior boundaries are etched even though the original grain is no longer present.

The misfit present at austenite grain boundaries can evidently be inherited in a fully transformed specimen. This is because the displacive transformation of austenite involves a minimal movement of atoms. The Bain Strain, which is the pure component of the deformation which converts the austenite lattice into that of ferrite, does not rotate any plane or direction by more than about 11° [100]. Furthermore, the change in volume during transformation is a few percent. The excellent registry between the parent and product lattices is illustrated by the electron diffraction pattern of Fig. 27.

Consequently, the detailed arrangement of atoms at an austenite grain boundary is unlikely to be influenced greatly by displacive phase transformation.

Widmanstätten ferrite – MECHANICAL PROPERTIES

There are many investigations which suggest that Widmanstätten ferrite can be detrimental to toughness [101–110]. Recent work involving controlled experiments has, however, established that when the microstructure is changed from one which is predominantly allotriomorphic ferrite, to one containing Widmanstätten ferrite, there is an improvement in both the toughness and strength [111]. This might be expected since large fractions of Widmanstätten ferrite are usually associated with refined microstructures.

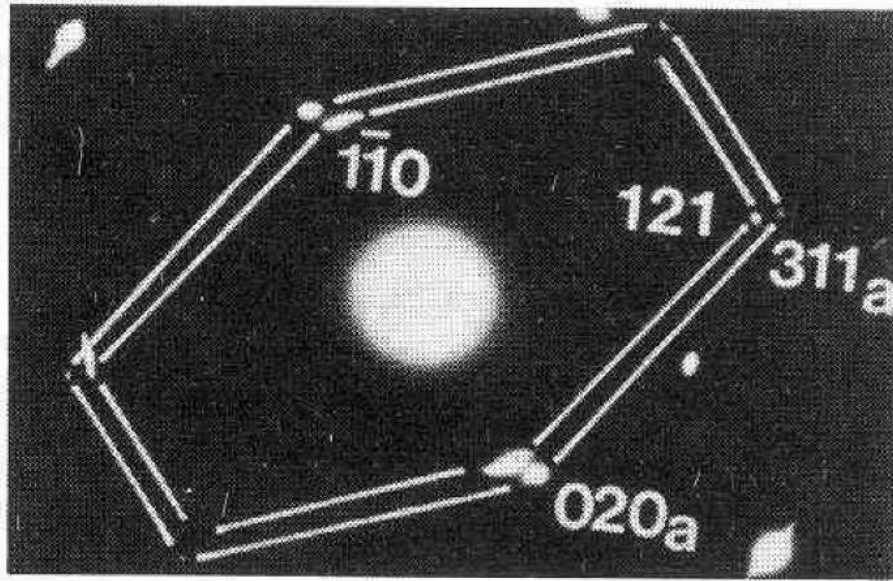


Fig. 27: Electron diffraction pattern from martensite and austenite in steel [40].

It is sometimes claimed that the presence of Widmanstätten ferrite changes the deformation behaviour by inducing continuous yielding during tensile deformation, whereas discontinuous yielding is characteristic of microstructures dominated by allotriomorphic ferrite. However, some careful studies by Bodnar and Hansen [111] show that even microstructures containing Widmanstätten ferrite often show discontinuous yielding behaviour. They suggested that in cases where continuous yielding has been reported, the microstructures contained sufficient quantities of bainite or martensite to mask the deformation behaviour of Widmanstätten ferrite.

ACICULAR FERRITE: MECHANISM OF TOUGHENING

An acicular ferrite microstructure is usually assumed to be good for the achievement of a high cleavage toughness. This is because the plates of ferrite point in many different directions, and hence are able to frequently deflect cracks. This should give better toughness when compared with allotriomorphic ferrite, or even Widmanstätten ferrite or bainite, which tends to form in packets of parallel plates (across which cracks can propagate with relative ease). However, good evidence to this latter effect has been lacking. An example is illustrated in Fig. 28, where the fracture assessed impact transition temperature is plotted as a function of the strength and microstructure [112]. It is obvious that the progressive replacement of a coarse allotriomorphic ferrite microstructure with acicular ferrite, even though the strength increases in the process.

As acicular ferrite is then replaced with bainite, the toughness deteriorates, but the cause of this is not straightforward to interpret because the strength increases at the same time (Fig. 28).

Similar observations have recently been reported for both wrought steel and for weld metal [113]. The data presented in Fig. 29 demonstrate again the fact that an acicular ferrite microstructure is desirable even though non-metallic inclusions have to be added in order to provide intragranular nucleation sites.

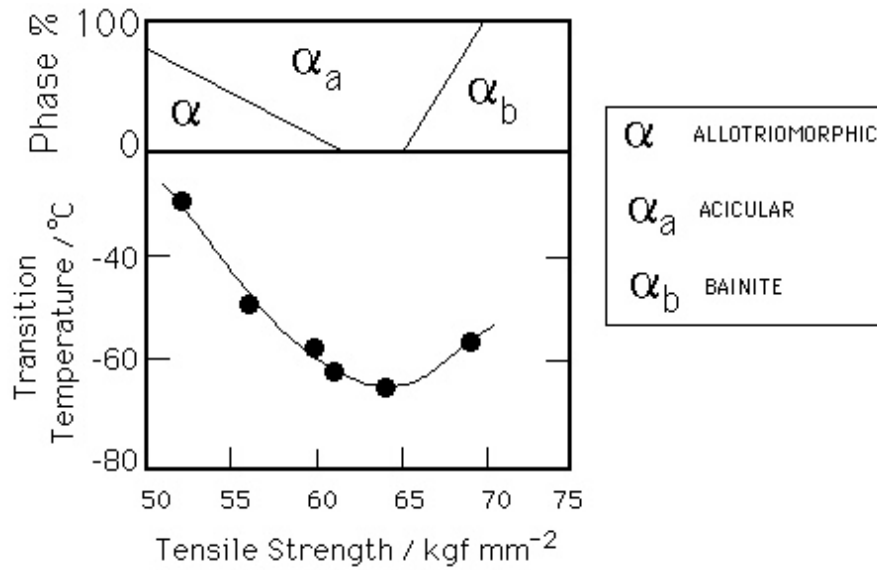


Fig. 28: Variation in the fracture assessed impact transition temperature as a function of the strength of the weld, and of the microstructure [112].

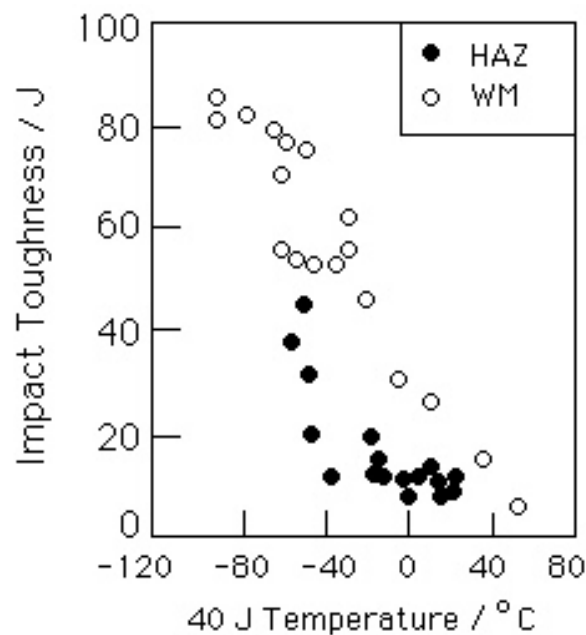


Fig. 29: Variation in the 40 J impact transition temperature as a function of the quantity of acicular ferrite in the microstructure [113]. The terms *HAZ* and *WM* represent the heat-affected zone and weld metal respectively.

Knott and co-workers have suggested that once a crack is initiated at an inclusion, it propagates without hindrance by acicular ferrite. Recent work by Ishikawa and Haze [114] has demonstrated that whilst this must be true when the general level of toughness is small, the gradient of stress at any position in the vicinity of a crack decreases as the toughness increases. Hence, the

propagation behaviour changes, and cleavage cracks are then arrested in an acicular ferrite microstructure but not in one which is dominated by Widmanstätten ferrite.

THE MICROPHASES

“Microphase” is the term used to describe the small amount of martensite, austenite, degenerate-pearlite which forms after all the other phases (allotriomorphic ferrite, Widmanstätten ferrite, acicular ferrite) have formed. The fraction of the microstructure which is left untransformed after the major phases have formed is very small in most low-alloy low-carbon steels; hence the term microphases. Microphases are also found in the heat-affected zones of welded steels.

The chemical composition of the microphases is for the substitutional solutes, identical to that of the alloy as a whole, but is substantially enriched with respect to the carbon concentration [115,116; Fig. ??]. The excess carbon is due to partitioning as the major phases grow. It is interesting (Fig. ??) that the degree of carbon enrichment is found to increase as the cooling rate decreases. This is because as the cooling rate decreases, the volume fraction of ferrite that grows prior to microphase formation is larger. Hence, by mass balance, the carbon concentration of the residual austenite is expected to be larger.

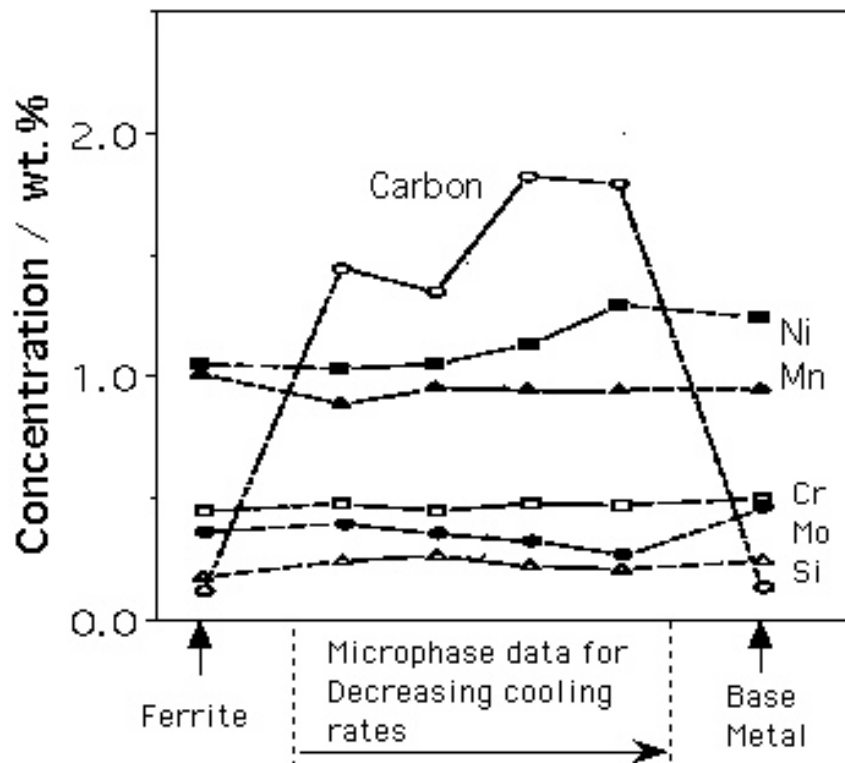


Fig. 30: The distribution of alloying elements in ferrite, the base metal and in the microphases, as a function of the cooling conditions. [116].

Fracture due to Microphases

It is generally recognised that microphases occur in two main morphologies, those originating from films of austenite which are trapped between parallel plates of ferrite, and others which are blocky in appearance.

The mechanism by which the microphases influence toughness in low-alloy steels (strength about 800 MPa) have been studied in detail by Chen *et al.* [117]. The effects vary with the test temperature. The films of hard phases tend to crack readily when loaded along their longest dimensions, often splitting into several segments. The blocks of microphases, on the other hand, tend to remain uncracked. At high temperatures, the cracks in the films initiate voids and hence lead to a reduction in the work of ductile fracture. The ferrite, which is softer and deforms first, has a relatively low strength at high temperatures and cannot induce fracture in the blocky microphases. The latter only come into prominence at low temperatures, where their presence induces stresses in the adjacent ferrite, stresses which peak at some distance ahead of the microphase/ferrite interface. This induces cleavage in the ferrite. Larger blocks are more detrimental in this respect because the peak stress induced in the adjacent ferrite is correspondingly larger.

SCATTER IN MECHANICAL PROPERTIES

Fracture mechanics are widely applied in the design of engineering structures, but difficulties arise when repeated tests of the kind used in characterising toughness, on the same material, yield significantly different results. Such scatter in toughness is a common feature of relatively brittle materials such as ceramics, where it is a key factor limiting their wider application even when the average toughness may be acceptable. Steel users have become increasingly aware in recent years that scatter in toughness data can also be of concern in wrought and welded steels. Apart from the difficulties in adopting values for design purposes, the tests necessary for the characterisation of toughness as a material property are rather expensive, the number of experiments needed to establish confidence being larger for less unreliable materials.

A major factor responsible for variations in toughness in welds is likely to be the inclusion population which consists mainly of large oxides originating from the slags used to control the weld pool stability and composition. The inclusions are neither uniform in size, nor are they uniformly distributed in the weld. There is also mounting evidence that variations in microstructure can also be an important factor in influencing scatter in toughness data [118–122]. Neville [123] noted that microstructural inhomogeneities such as hard pearlite islands, can lead to a significant variations in measured fracture toughness values during repeat tests on specimens of the same material.

The two quantities that need to be defined in order to assess variations in mechanical properties are the degree of scatter, and the heterogeneity of microstructure. The definitions have to be of a kind amenable to alloy design techniques, while at the same time being physically meaningful.

Representation of Scatter

Consider the scatter commonly observed in impact toughness data. The three most frequently used ways of rationalising variations in results from the toughness testing of weld metals are to take an average of the Charpy readings obtained at a given temperature, measure the standard deviation [124], or plot the lowest Charpy readings obtained in order to focus attention on the lower ends of the scatter bands [125].

An alternative to this was suggested by Smith [126] who proposed a scatter factor SF to quantify any spread obtained in Charpy values, where

$$SF = \frac{\text{Maximum Energy} - \text{Minimum Energy}}{\text{Average Energy}} \times 100(\%) \quad (22)$$

This is essentially a definition of *range*. As such, it has the disadvantage of giving excessive weight to the extreme values, taking account of all intermediate results only via the mean in the denominator. The relation is in general an unpredictable function of test temperature.

None of the methods discussed above are completely suitable for alloy design purposes, where the aim is to minimise scatter over the whole of the impact transition curve (the plot of impact energy versus test temperature). An idealised impact energy–temperature curve should be sigmoidal in shape, and the scatter of experimental data can in principle be measured as a root–mean–square deviation about a such a curve, obtained by best–fitting to the experimental data. This gives a representation of scatter in which one value of scatter is defined for each complete impact transition curve. It has the advantage that the value represents the entire dataset used in generating the transition curve.

Representation of Microstructural Heterogeneity

Since it is believed that the scatter in Charpy data is amongst other factors, dependent on the nonuniformity of weld microstructure, the degree of inhomogeneity needs to be quantified. This can be done by calculating the entropy H of a given microstructure [127,128].

If X is a random variable assuming the value i with probability p_i , $i = 1, \dots, n$, the entropy of X , as a logarithmic measure of the mean probability, is computed according to

$$H\{X\} = - \sum p_i \ln\{p_i\}. \quad (23)$$

It should be noted that for $p_i = 1$, $H\{X\} = 0$. Conversely, the entropy is a maximum value $\ln\{n\}$ when $p_1 = \dots = p_n = \frac{1}{n}$.

The primary microstructure of most common welds can be taken as having three principal constituents: acicular, allotriomorphic and Widmanstätten ferrite. It is important to emphasise that although α_a and α_w have similar strengths, the weld metal microstructure cannot be treated as a two–phase microstructure (with α_a and α_w grouped together), since the *toughness values* of the two phases are quite different. Therefore, the entropy of a given weld metal microstructure

$$H = -[V_\alpha \ln\{V_\alpha\} + V_a \ln\{V_a\} + V_w \ln\{V_w\}] \quad (24)$$

where V_α , V_a and V_w are the volume fractions of allotriomorphic, acicular and Widmanstätten ferrite respectively.

The entropy of the distribution quantifies the heterogeneity of the microstructure. H will vary from zero for an homogeneous material to $\ln\{3\}$ (*i.e.* 1.099) for a weld with equal volume fractions of the three phases. By multiplying by $1/\ln\{3\}$, the heterogeneity of the three phase microstructure of a weld may be defined on a scale from zero to unity, *i.e.*

$$Het_3 = H \times 0.910. \quad (25)$$

Another scale of heterogeneity can also be addressed, to see if the primary and secondary regions of multipass welds could be treated similarly. Here, the secondary region is taken to comprise that part of the microstructure consisting of partially re-austenitised and significantly tempered regions [57]. It follows that the heterogeneity of the assumed two-phase microstructure is given by

$$Het_2 = -[V_p \ln\{V_p\} + V_s \ln\{V_s\}] \times \frac{1}{\ln\{2\}} \quad (26)$$

where V_p and V_s are the volume fractions of the primary and secondary regions respectively.

It is evident from (Fig. 31a) that there is a strong relationship between the scale parameter, and microstructural heterogeneity for low-alloy steel all-weld metals. Consequently, a significant part of the observed scatter in weld metal Charpy results is attributable to the inhomogeneity of the microstructure, with larger scatter being associated empirically with more heterogeneous microstructures. This result can be compared with the common feature of fracture toughness experiments where the positioning of the fatigue crack is found to be an important factor in CTOD testing of weldments.

EFFECT OF COPPER

Copper has two primary effects, firstly to retard the transformation of austenite (since it is an austenite stabilising element), and secondly to strengthen ferrite via the precipitation of ϵ -Cu.

In manual metal arc welds, copper increases the strength, but at concentrations in excess of about 0.7 wt.% to a deterioration in toughness in both the as-welded and stress-relieved states [129]. There may be a simple explanation for this, in that an increase in strength should indeed lead to a deterioration of toughness, since the comparisons are never at constant strength.

Kluken *et al.* [85] showed that in submerged arc welds, the yield strength is less sensitive to copper additions than the ultimate tensile strength, perhaps because the copper precipitates cause a greater rate of work hardening. On the other hand, Es-Souni *et al.* [129] found the rate of change, as a function of the copper concentration, to be identical for both the yield and tensile strengths, in manual metal arc welds.

The austenite stabilising effect of copper seems to cause either an increase in the microphase content, or changes the nature of the microphases from cementite and ferrite to mixtures of

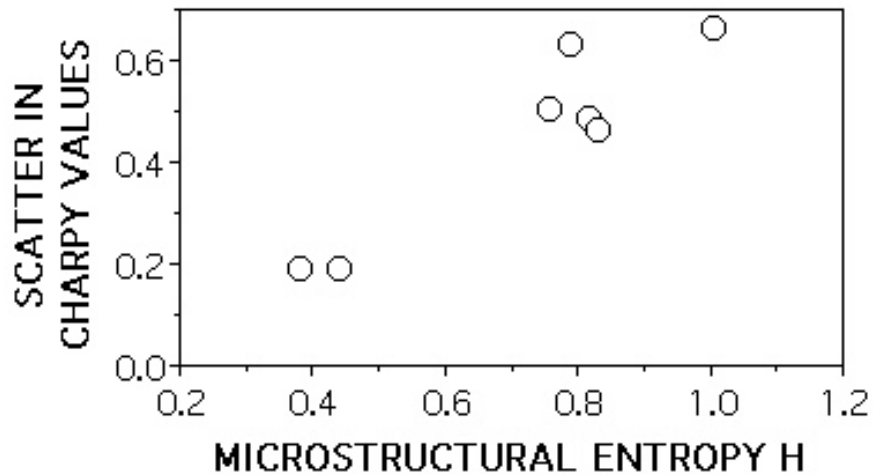


Fig. 31: The relationship between microstructural heterogeneity and scatter, as measured by the scale parameter. Each point corresponds to a calculation using a complete Charpy impact transition curve.

retained austenite and high-carbon martensite [129,130]. The presence of copper has not been found to influence either the distribution or the nature of the usual non-metallic inclusions found in steel weld deposits [129].

HYDROGEN REMOVAL AND IRREVERSIBLE PROCESSES

Hydrogen is a key parameter controlling the mechanical properties of welded assemblies. There has been a fascinating development on the methods available for the directional removal of hydrogen following a welding operation. It is, however, necessary to describe first some background theory to set the idea into context.

In all our discussions of thermodynamics, we have dealt with measurable properties of materials, formulated on the concept of equilibrium. There are, however, many properties of nonequilibrium systems (thermal conductivity, diffusion, viscosity *etc.*) which are similar to thermodynamic properties, such as temperature, density or entropy, in that their definitions are not based on the structure of matter. Nonequilibrium thermodynamics, or the thermodynamics of irreversible processes deals with the relations between such properties [131,132].

Reversibility

Classical thermodynamics only applies to systems which are in equilibrium. A reversible process is one which can be reversed by an infinitesimal change in the external conditions [133]. If we consider the motion of a piston in a cylinder containing a compressible fluid, the reversible motion of the piston in the cylinder would lead to a pressure-volume relation illustrated by the light curve of Fig. 32. Any friction to the motion of the piston would make the process

irreversible since an infinitesimal application of force would not move that piston. Energy (given by the area within the bold loop of Fig. 32) would therefore be dissipated during the cyclic frictional motion of the piston, a key feature of irreversible processes.

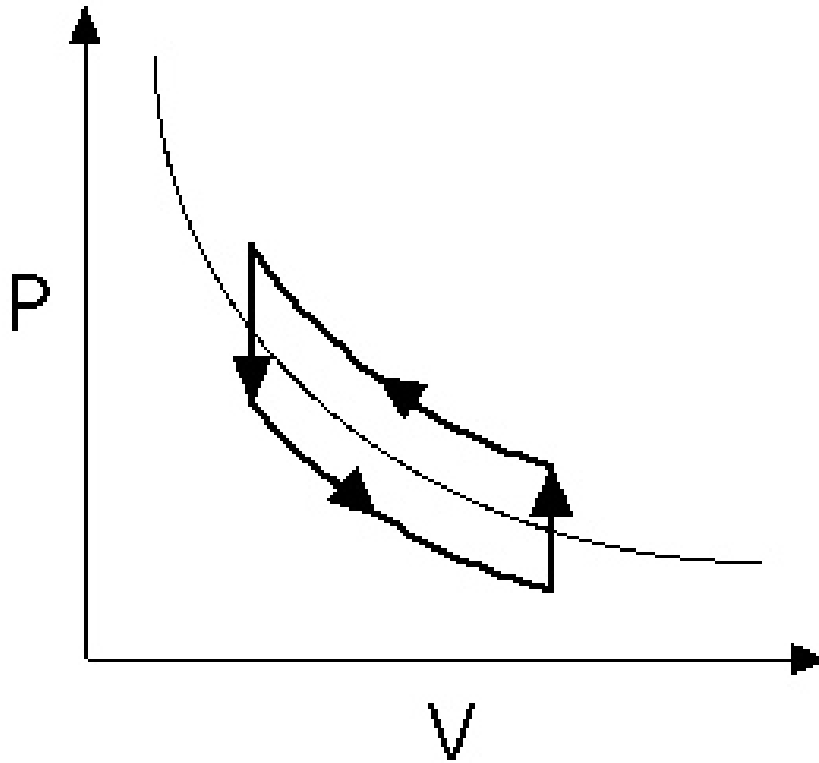


Fig. 32: Effect of friction on the pressure (P) versus volume (V) relation for a compressible fluid. The light curve represent the case without friction, whereas the bold loop is when there is frictional resistance to the motion of the piston.

More generally then, reversibility means that one can pass from one state to another without appreciable deviation from equilibrium. Most real process are, therefore, not reversible. For irreversible processes the *equations* of classical thermodynamics become *inequalities*. For example, at the equilibrium melting temperature, the free energies $G_{liquid} = G_{solid}$ but below the melting temperature, $G_{liquid} > G_{solid}$. Such inequalities are much less useful and provide information only about the direction of likely change.

There is however, some rough (kinetic) theory which can allow us to relate the magnitude of the inequality to the rate of change. Such theory is controversial in an interesting sense, and lacks generality [131]. The assumptions involved must be verified experimentally. On the other hand, once backed by experiment, quantitative deductions and predictions become possible.

The Linear Laws

At equilibrium there is no change in entropy or free energy. For any irreversible process, there is energy dissipated. In the above example, it is the heat that is created by friction that leads to

dissipation of energy and the creation of entropy. The energy dissipation rate can be expressed as the product of the temperature and rate of entropy production ($T\sigma$). The dissipation is always found to be of the form:

$$T\sigma = JZ \quad (27)$$

where J is a “flux” of some kind, and Z a “force”. The rate of heat dissipation when a current flows is given by the product of the current (the flux) and the electromotive force (e.m.f., the force).

A major result of kinetic theory for nonequilibrium processes is that forces and their conjugate fluxes are linearly related whenever the above equation applies.

The force may be a chemical driving force (ΔG), an electromotive force (e.m.f.) (V), a thermal gradient $\frac{1}{T} \frac{dT}{dz}$ etc. The corresponding fluxes might be interface velocity (V_I), electrical current (I) and heat diffusion (J_H) respectively.

$$V_I = M\Delta G \quad (28)$$

$$I = \frac{1}{R}V \quad (29)$$

$$J_H = -\frac{K}{T} \frac{dT}{dz} \quad (30)$$

Multiple Irreversible Processes

Many irreversible processes acting together can easily be handled, because the total energy dissipation rate is simply

$$T\sigma = \sum_i J_i Z_i. \quad (31)$$

We can therefore consider diffusion under the influence of both a concentration gradient and an electrical field, as in electromigration.

For more than one irreversible process, it is found experimentally that each flow J_i is related not only to its conjugate force Z_i , but is also linearly related to all other forces present. Thus,

$$J_i = M_{ij} Z_j \quad (32)$$

with $i, j = 1, 2, 3, \dots$

Solute diffusion can therefore be expressed as a function of both the chemical potential gradient and the e.m.f. as follows:

$$J_D = -M_{11} \nabla \mu - M_{12} \nabla V \quad (33)$$

where μ is the chemical potential of the solute and J_D is the diffusion flux. Mishra *et al.* [134] have recently applied this equation to the diffusion of hydrogen in welded assemblies, with the aim of removing the hydrogen by applying an e.m.f. across the assembly instead of the conventional procedure which involves a post-weld heat treatment. They find that at ambient temperature, an electrical field of just 0.1 volts per cm when applied to the joint for 30 minutes (Fig. 33) is sufficient to remove 50% of the hydrogen from starting concentration of 5 parts per million. This process has been dubbed *post-weld electrotransport treatment* and possibly represents the most novel idea on the subject of hydrogen in welds for many a year. It has the possibility of reducing hydrogen susceptibility without heat treatment.

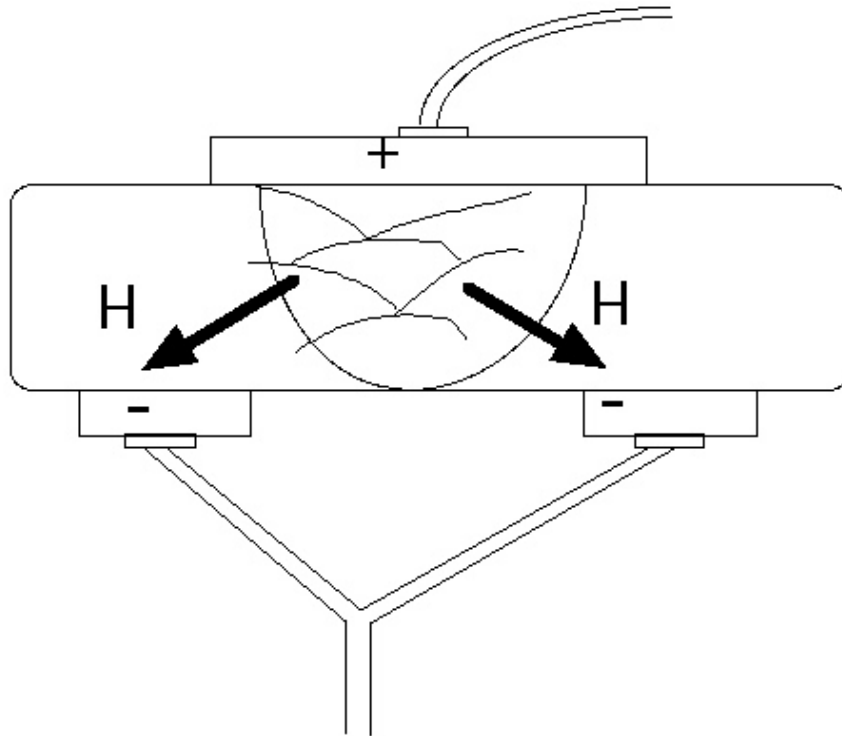


Fig. 33: Schematic method for post-weld electrotransport treatment for hydrogen removal [134].

DESTRUCTIVE METALLURGY

There is an example in processing where hydrogen is used to induce the disintegration of a material. In the hydrogen decrepitation process, sintered solids are charged with hydrogen, causing them to crumble, thus producing the desired powder for further processing [135,136]. The process is used for making sintered magnets. It would be interesting to exploit such metallurgical phenomena to help in the catastrophic or gradual destruction of large steel structures.

Obsolete oil rigs are massive steel structures which have to be decommissioned safely. Some rigs are disposed by using explosives to sever them into two parts, both of which are sunk into the ocean, taking care to leave about 55 m of clear water above the sunken components for free navigation. It would be an advantage if these large sunken segments could deteriorate

quickly into much smaller segments on the ocean floor. One possibility is to charge localised regions of the rigs with hydrogen, so that hydrogen cracking then leads to further underwater disintegration of the large segments over a short period of time after the sinking. Bead-on-plate welds could be deposited at critical nodes, the welding being carried out using electrodes which have a high carbon concentration and a number of water-containing minerals. This would lead to a hard deposit with a great deal of hydrogen, thus not only charging the underlying rig-steel with hydrogen but also providing sharp cracks in the weld which can then propagate into the substrate. It may be the case that self-stress in the rig would then be sufficient to permit the large scale propagation of cold-cracks.

CONCLUSIONS

Microstructural models are in many cases sufficiently advanced to give accurate predictions for welds. It is now necessary to focus attention on the relationship between microstructure and mechanical properties, so that data useful as design parameters can easily be generated.

It has been demonstrated here that both simple and complex mechanical properties can be modelled with considerable success if appropriate modelling techniques are used. Parameters such as strength have a firm foundation in metallurgy and can indeed be estimated using known metallurgical principles. Others such as toughness are less amenable to fundamental analysis but can nevertheless be modelled using pattern recognition methods. A great deal of work remains to be done before comprehensive models for all the desired properties can be constructed; a priority list of the properties which need analysis is presented in Table 4.

Property	Relevance
Yield strength	All structural applications
Ultimate tensile strength	All structural applications
YS/UTS ratio	Tolerance to plastic overload
Elongation	Resistance to brittle fracture
Uniform elongation	Related to YS and UTS
Non-uniform elongation	Related to inclusion or precipitate content
Toughness	Tolerance to defects
Fatigue	Cyclic loading, life assessments
Stress corrosion	Slow crack growth in corrosive environment
Creep strength	High temperature service
Creep ductility	Safe design
Creep-fatigue	Fatigue at creep temperatures
Elastic modulus	Deflection, stored energy
Thermal expansion coefficient	Thermal fatigue
Hardness	Tribological properties

Table 4: Mechanical properties of steel welds and their main relevance.

ACKNOWLEDGMENTS

I am grateful to Colin Humphreys for his continuing support of my research and also sincerely acknowledge the long term support of welding research by Dr. Lars-Erik Svensson of ESAB AB (Sweden). The Engineering and Physical Sciences Research Council provided some financial support over the years.

REFERENCES

- 1, (Alberly, P. J. and Jones, W. K. C.) 1979 *CEGB report R/M/R282, Marchwood Engineering Laboratories, Marchwood, Southampton, U. K.*
- 2, (Alberly, P. J. and Jones, W. K. C.) 1982 **Metals Technology**, 9, 419–427.
- 3, (Alberly, P. J., Brunnstrom, R. R. L. and Jones, K. E.) 1983 **Metals Technology**, 10, 28–38.
- 4, (Ashby, M. F. and Easterling, K. E.) 1982 **Acta Metallurgica**, 30, 1969–1978.
- 5, (Ion, C., Easterling, K. E. and Ashby, M. F.) 1984 **Acta Metallurgica**, 32, 1949–1962.
- 6, (Goldak, J., Chakravarti, A. and Bibby, M.) 1984 **Metallurgical Transactions B**, 15B, 299–305.
- 7, (Goldak, J., Bibby, M., Moore, J., House, R. and Patel, B.) 1986 **Metallurgical Transactions B**, 17B, 587–600.
- 8, (Bhadeshia, H. K. D. H.) 1989 *Recent Trends in Welding Science and Technology*, eds. S. A. David and J. M. Vitek, ASM International, Ohio, U. S. A., 189–198.
- 9, (Bhadeshia, H. K. D. H.) 1990 **Metallurgy, Welding and Qualification of Microalloyed (HSLA) Steel Weldments**, eds. J. T. Hickey, D. G. Howden and M. D. Randall, American Welding Society, Florida, U.S.A., 34–69
- 10, (Bhadeshia, H. K. D. H. and Svensson, L.–E.) 1993 **Mathematical Modelling of Weld Phenomena**, eds. H. Cerjak and K. E. Easterling, Institute of Materials, London, 109–182.
- 11, (Olson, D. L., Liu, S. and Edwards, G. R.) 1993 **Mathematical Modelling of Weld Phenomena**, eds. H. Cerjak and K. E. Easterling, Institute of Materials, London, 89–108.
- 12, (Grong, ϕ .) 1995 **Metallurgical Modelling of Welding**, Institute of Materials, London, 1–600.
- 13, (Bhadeshia, H. K. D. H.) 1995 **Mathematical Modelling of Weld Phenomena 2**, eds. H. Cerjak and H. K. D. H. Bhadeshia, Institute of Materials, London, 71–118.
- 14, (Kranszberg, M. and Smith, C. S.) 1979 **Materials Science and Engineering**, 37,30.
- 15, (Radaj, D.) 1995 **Mathematical Modelling of Weld Phenomena 2**, eds. H. Cerjak and H. K. D. H. Bhadeshia, Institute of Materials, London, 245–264.
- 16, (Leslie, W. C.) 1982 **Physical Metallurgy of Steels**, McGraw–Hill Kogakusha, Tokyo, Japan.
- 17, (Conrad, H. and Fredrick, S.) 1962 **Acta Metallurgica**, 10,1013–1020.
- 18, (Altshuler, T. L. and Christian, J. W.) 1967 **Proceedings of the Royal Society**, 261A,253–287.
- 19, (Kimura, H., Matsui, H., Takaki, S., Kimura, A. and Oguri, K.) 1981 **Mechanical Properties of BCC Metals**, ed. M. Meshii, The Metallurgical Society of AIME, Warrendale, Pennsylvania, 125–133.
- 20, (Bhadeshia, H. K. D. H.) 1992 **Bainite in Steels**, Institute of Materials, London, 1–458.
- 21, (Hultgren, A.) 1951 **Jernkontorets Ann.**, 135, 403.
- 22, (Hillert, M.) 1952 **Jernkontorets Ann.**, 136, 25–37.
- 23, (Bhadeshia, H. K. D. H.) 1985 **Progress in Materials Science**, 29, 321–386.
- 24, (Leslie, W. C.) 1972 **Metallurgical Transactions**, 3,5–26.
- 25, (Takeuchi, S.) 1969 **Journal of the Physical Society of Japan**, 27,929–940.

- 26, (Honeycombe, R. W. K. and Bhadeshia, H. K. D. H.) 1995 **Steels, Microstructure and Properties**, 2nd edition, Edward Arnold, London.
- 27, (Svensson, L.-E.) 1994 **Control of Microstructure and Properties in Steel Arc Welds**, CRC Press, London.
- 28, (Bhadeshia, H. K. D. H.) 1982 **Metal Science**, 16, 167–169.
- 29, (Abiko, K.) June 1993 **Scientific American**, Japanese edition, 20–29.
- 30, (Maki, T.) 1994 **Physical Metallurgy of IF Steels**, Iron and Steel Institute of Japan, Tokyo, 183–197.
- 31, (Christian, J. W.) 1971 **Strengthening Methods in Crystals**, eds. A. Kelly and R. Nicholson, Elsevier, North-Holland, 261–329.
- 32, (Christian, J. W.) 1979 **Proceedings of an International Conference on Martensitic Transformations, ICOMAT '79**, M.I.T. press, Cambridge, Massachusetts, U.S.A., 220–234.
- 33, (Takahashi, M. and Bhadeshia, H. K. D. H.) 1990 **Materials Science and Technology**, 6 592–603.
- 34, (Young, C. H. and Bhadeshia, H. K. D. H.) 1994 **Materials Science and Technology**, 10,209–214.
- 35, (Yang J. R. and Bhadeshia, H. K. D. H.) 1990 *The Dislocation Density of Acicular Ferrite in Steel Welds*, **Welding Journal Research Supplement**, 69,305s–307s.
- 36, (Langford, G. and Cohen, M.) 1969 **Trans. ASM**, 62,623.
- 37, (Langford, G. and Cohen, M.) 1970 **Metallurgical Transactions**, 1,1478–1480.
- 38, (Wechsler, W. S., Lieberman, D. S. and Reed, T. A.) 1953 **Trans. AIMME**, 197,1503–1515.
- 39, (Bowles, J. S. and MacKenzie, J. K.) 1954 **Acta Metallurgica**, 2,129–234.
- 40, (Bhadeshia, H. K. D. H.) 1987 **Worked Examples in The Geometry of Crystals**, Institute of Metals, London.
- 41, (Olson, G. B. and Cohen, M.) 1981 **Solid→Solid Phase Transformations**, eds. H. I. Aaronson *et al.*, TMS–AIME, Warrendale, Pennsylvania, USA, 1209.
- 42, (Kelly, P. M. and Pollard, G.) 1969 **Acta Metallurgica**, 17,1005.
- 43, (Tomita, Y. and Okabayashi, K.) 1983 **Metallurgical Transactions A**, 14A,485–492.
- 44, (Tomita, Y. and Okabayashi, K.) 1983 **Metallurgical Transactions A**, 14A,2387–2393.
- 45, (Tomita, Y. and Okabayashi, K.) 1985 **Metallurgical Transactions A**, 16A,73–82.
- 46, (Tomita, Y. and Okabayashi, K.) 1985 **Metallurgical Transactions A**, 16A,83–91.
- 47, (I. Hrivnak) 1996 **Mathematical Modelling of Weld Phenomena 3**, eds. H. Cerjak, B. Buchmayer and H. K. D. H. Bhadeshia, Institute of Materials, London, in press.
- 48, (Christian, J. W.) 1958 **Acta Metallurgica**, 6,377–379.
- 49, (Kurdjumov, G. V. and Khandros, L. G.) 1949 **Dokl. Akad. Nauk SSSR**, 66,221.
- 50, (Olson, G. B. and Cohen, M.) 1977 **Scripta Metallurgica**, 11,345–347.
- 51, (Salzbrenner, R. J. and Cohen, M.) 1979 **Acta Metallurgica**, 27,739–748.
- 52, (Court, S. and Pollard, J.) 1987 **Welding Metallurgy of Structural Steels**, ed. J. Y. Koo, TMS–AIME, Pennsylvania, 335–349.
- 53, (Zhang, Zhu Yau) 1994 **Ph.D. Thesis**, Southampton University.
- 54, (Chang, L. C. and Bhadeshia, H. K. D. H.) 1995 **Materials Science and Technology**, in press.

-
- 55, (Sugden, A. A. B. and Bhadeshia, H. K. D. H.) 1988 **Metallurgical Transactions A**, 19A,1597–1602.
- 56, (Svensson, L.–E. and Bhadeshia, H. K. D. H.) 1988 *Improved Weldment Control using Computer Technology, Vienna, Austria, Pergamon Press, Oxford*, 71–78.
- 57, (Svensson, L.–E., Grefott, B., Sugden, A. A. B. and Bhadeshia, H. K. D. H.) 1988 **Computer Technology in Welding II, Welding Institute, Abingdon, UK**, paper 24.
- 58, (Jones, B. L. and Johnson, D. L.) 1983 **Steels for Line–Pipe and Pipeline Fittings**, Metals Society, London, 14.
- 59, (Sugden, A. A. B. and Bhadeshia, H. K. D. H.) 1989 **J. Materials Science**, 25, 613–618.
- 60, (Knott, J. F.) 1995 **Micromechanisms of Fracture and Their Structural Significance**, Second Griffith Conference, Institute of Materials, London, 3–14.
- 61, (McMahon Jr., C. J. and Cohen, M.) 1965 **Acta Metallurgica**, 13,591.
- 62, (D. A. Curry and J. F. Knott) 1978 **Metal Science**, 12,511.
- 63, (Wallin, K.) 1993 **International Journal of Pressure Vessels and Piping**, 55,61–79.
- 64, (Wallin, K.) 1995 **Micromechanisms of Fracture and Their Structural Significance**, Second Griffith Conference, Institute of Materials, London, 131–140.
- 65, (Knott, J. F.) 1973 **Fundamentals of Fracture Mechanics**, Butterworths, London, 8.
- 66, (Akselsen, O. M. and Grong, ϕ .) 1992 **Materials Science and Engineering A**, A159, 187–192.
- 67, (MacKay, D. J. C.) 1992a **Neural Computation**, 4, 415–447.
- 68, (MacKay, D. J. C.) 1992b **Neural Computation**, 4, 448–472.
- 69, (Bhadeshia, H. K. D. H., Svensson, L.–E. and Mackay, D. J. C.) 1995 **Materials Science and Technology**, in press.
- 70, (Lau, T. W., Sadowsky, M. M., North, T. H. and Weatherly, G. C.) 1987 **Welding Metallurgy of Structural Steels**, ed. J. Y. Koo, T.M.S.–A.I.M.E., Warrendale, Pennsylvania, U.S.A., 349–365.
- 71, (Lau, T. W., Sadowsky, M. M., North, T. H. and Weatherly, G. C.) 1988 **Materials Science and Technology**, 4, 52–61.
- 72, (Oldland, R. B.) December 1985 **Australian Welding Research**, 31–43.
- 73, (Ahlblom, B., Bergstrom, U., Hannerz, N. E. and Werlefors, I.) 1986 *WI conference on Residuals and Impurities in Steels* Welding Institute, Abington, Cambridge, U. K., paper 49
- 74, (Grong, ϕ , Kluken, A. O. and Bjornbakk, B.) 1988 **Joining and Materials**, 1, 164–169.
- 75, (Liou, H. Y., Liao, C. M. and Wang, S. C.) 1992 **China Steel Technical Report No. 6**, 30–37.
- 76, (Evans, G. M.) 1980 **American Welding Journal**, 59, 67s–75s.
- 77, (Svensson, L.–E. and Grefott, B.) 1990 **American Welding Journal**, 69, 454s–461s.
- 78, (Abson, D. J.) 1988 *Welding Institute Research Report 376/1988, Cambridge, UK*.
- 79, (Still, J. R. and Rogerson, J. H.) 1978 **Metal Construction**, 10, 339–342.
- 80, (Still, J. R. and Rogerson, J. H.) 1980 **Metal Construction**, 12, 120–123.
- 81, (Kluken, A. O. and Grong, ϕ) 1992 *Temper embrittlement in steel weld metals containing titanium and boron* **International Trends in Welding Science and Technology** eds. S. A. David and J. M. Vitek, ASM International, Metals Park, Ohio, U. S. A., 569–574.

- 82, (Kayali, E. S., Pacey, A. J. and Kerr, H. W.) 1984 **Canadian Metallurgical Quarterly**, 23,227–236.
- 83, (Lazor, R. B. and Kerr, H. W.) 1980 *Pipeline and Energy Plant Piping: Design and Technology*, Pergamon Press, Toronto, Canada, 141–149.
- 84, (Sneider, G. and Kerr, H. W.) 1984 **Canadian Metallurgical Quarterly**, 23, 315–325.
- 85, (Kluken, A. O., Siewert, T. A. and Smith, R.) 1994 *Effects of copper, nickel and boron on mechanical properties of low-alloy steel weld metals deposited at high heat input* **American Welding Journal**, 73, 193s–199s.
- 86, (Ichikawa, K., Horii, Y., Motomatsu, R., Yamaguchi, M. and Yurioka, N.) 1994 **Quarterly Journal of the Japan Welding Society**, in press.
- 87, (Iezawa, T., Inoue, T., Hirano, O., Okazawa, T. and Koseki, T.) 1993 **Tetsu to Hagane**, 79,96–102.
- 88, (Briant, C. L. and Banerji, S. K.) 1978 **International Metals Reviews**, 232, 164–199.
- 89, (Schulz, B. J. and McMahan Jr., C. J.) 1972 **Temper Embrittlement of Alloy Steels**, STP 499, American Society for Testing and Metals, 104.
- 90, (McMahan Jr., C. J., Cianelli, A. K., Feng, H. C. and Ucisik, A. H.) 1977 **Metallurgical Transactions A**, 8A, 1059.
- 91, (Yu, J. and McMahan Jr., C. J.) 1980 **Metallurgical Transactions A**, 11A, 291.
- 92, (McMahan Jr., C. J. and Qu Zhe) 1983 **Metallurgical Transactions A**, 14A, 1101.
- 93, (Krauss, G. and McMahan Jr., C. J.) 1992 **Martensite**, eds. G. B. Olson and W. S. Owen, ASM International, Materials Park, Ohio, U.S.A., 295–322.
- 94, (Steven, W. and Balajiva, K.) 1959 **J. Iron and Steel Institute**, 193, 141.
- 95, (Yu-Qing, W. and McMahan Jr., C. J.) 1986 **Supplement to Trans. Japan Inst. Metals**, 27, 579.
- 96, (McMahan Jr., C. J.) 1987 **Innovations in ultrahigh-strength steel technology**, eds. G. B. Olson, M. Azrin and B. S. Wright, Sagamore Army Research Conference, Northwestern University, U.S.A., 597–618.
- 97, (Hyam, E. D. and Nutting, J.) 1956 **Journal of the Iron and Steel Institute**, 184,148–165.
- 98, (Baker, R. G. and J. Nutting) 1959 **Journal of the Iron and Steel Institute**, 192,257–268.
- 99, (Vander Vroot, G. F.) 1984 **Metallography, Principles and Practice**, McGraw-Hill Book Company, London, 219–223.
- 100, (Crosky, A., McDougall, P. G. and Bowles, J. S.) 1980 **Acta Metallurgica**, 28,1495–1504.
- 101, (Owen, W. S., Whitmore, D. H., Cohen, M. and Averbach, B. L.) 1957 **Welding Journal Research Supplement**, November, 503s–511s.
- 102, (Gulyaev, A. P. and Guzovskaya, M. A.) 1977 **Met. Sci. Heat Treat.**, 19, 1020–1024.
- 103, (Koval'chuk, G. Z., Geichenko, V. N., Yarmosh, V. N. and Podobedova, L. V.) 1979 **Met. Sci. Heat Treat.**, 21, 114–117.
- 104, (Chilton, J. M. and Roberts, M. J.) 1979 **Vanadium in High Strength Steels**, Vanitec, London, 11–21.
- 105, (Chilton, J. M. and Roberts, M. J.) 1980 **Metallurgical Transactions A**, 11A, 1711–1721.
- 106, (Otterberg, R., Sandrom, R. and Sandberg, A.) 1980 **Metals Technology**, 7, 397–408.

- 107, (Stenbacka, N.) 1980 **Scandinavian Journal of Metallurgy**, 9, 225–236.
- 108, (Morrison, W. B. and Preston, R. R.) 1984 **Proc. Int. Symp. on Niobium**, edited by H. Stuart, TMS–AIME, Warrendale, PA, 939–966.
- 109, (Glover, G., Oldland, R. B. and Voight, G.) 1984 **High–Strength, Low–Alloy Steels**, eds. D. P. Dunne and T. Chandra, South Coast Printers, New South Wales, Australia, 271–275.
- 110, (Huang, Z. and Yao, M.) 1989 **Materials Science and Engineering A**, A119, 211–217.
- 111, (Bodnar, R. L. and Hansen, S. S.) 1994 **Metallurgical and Materials Transactions A**, 25A, 763–773.
- 112, (Horii, Y. and Ohkita, S.) 1992 **Welding International**, 6, 761–765.
- 113, (Harrison, P. L. and Hart, P. H. M.) 1995 **Micromechanisms of Fracture and Their Structural Significance**, Second Griffith Conference, Institute of Materials, London, 57–68.
- 114, (Ishikawa, T. and Haze, T.) 1994 **Materials Science and Engineering A**, A176, 385–391.
- 115, (Komizo, Y. and Fukada, Y.) 1989 *CTOD properties and MA constituent in the HAZ of C–Mn Microalloyed Steel*, **The Sumitomo Search**, No. 40, 31–40.
- 116, (Matsuda, F., Li, Z., Bernasovsky, P., Ishihara, K. and Okada, H.) 1990 *An Investigation of the Behaviour of M–A constituent in Simulated HAZ of HSLA steels*, **IIW Document IX–B–1591–90**.
- 117, (Chen, J. H., Kikuta, Y., Araki, T., Yoneda, M. and Matsuda, Y.) 1984 **Acta Metallurgica**, 32, 1779–1788.
- 118, (Tweed, J. H. and Knott, J. F.) 1983 **Metal Science**, 17, 45–54.
- 119, (Tweed, J. H. and Knott, J. F.) 1987 **Acta Metallurgica**, 35, 1401–1414.
- 120, (Bowen, P., Druce, S. G. and Knott, J. F.) 1986 **Acta Metallurgica**, 34, 1121–1131.
- 121, (Neville, D. and Knott, J. F.) 1986 **J. Mechanics and Physics of Solids**, 34, 243–291.
- 122, (Hagiwara, Y. and Knott, J. F.) 1980 **Advances in Fracture Research**, ed. D. Francois, Pergamon Press, Oxford, U. K. 707.
- 123, (Neville, D.) 1985 *Ph.D. Thesis, University of Cambridge, U. K.*
- 124, (Drury, B. G.) 1984 **Welding and Metal Fabrication**, 53, 250–252.
- 125, (Taylor, D. S.) 1982 **Welding and Metal Fabrication**, 50, 452–460.
- 126, (Smith, E.) 1983 **Welding and Metal Fabrication**, 51, 210–204.
- 127, (Lange, F. H.) 1967 **Correlation Techniques**, Iliffe Books Ltd., London, U. K. 76–77.
- 128, (Karlin, S. and Taylor, H. M.) 1975 **A First Course in Stochastic Processes**, Academic Press, New York, U. S. A., 495–502.
- 129, (Es-Souni, M., Beaven, P. A. and Evans, G. M.) 1990 *Microstructure and mechanical properties of Cu–bearing MMA C–Mn weld metal* **Oerlikon Schweibmitteilungen**, No. 123, 15–31.
- 130, (Alekseev, A. A., Shevchenko, G. A., Pokhodnya, I. K. and Yurlov, B. V.) 1991 *Effect of copper on structure and properties of multilayer C–Mn–Ni weld metal* **IIW Document II–A–845–91**, 1–7.
- 131, (Christian, J. W.) 1975 *Theory of Transformations in Metals and Alloys, 2nd ed., Part I*, Pergamon Press, Oxford.
- 132, (Miller, D. G.) 1960 **Chemical Reviews**, 60,15–37.

- 133, (Pippard, A. B.) 1981 **The Elements of Classical Thermodynamics**, Cambridge University Press, Cambridge, U. K., 22.
- 134, (Mishra, B., Olson, D. L. and David, S. A.) 1995 **Journal of Materials Engineering and Performance**, 3,612–618.
- 135, (Harris, I. R.) 1985 **Journal of the Less–Common Metals**, 106,L1.
- 136, (Harris, I. R.) 1987 **Journal of the Less–Common Metals**, 131,245.